

Response to reviewer 1:

Thank you for your letter and valuable comments and questions concerning our manuscript entitled "Error analyses of a multistatic meteor radar system to obtain a 3-dimensional spatial resolution distribution" [MS no. amt-2020-353]. These comments are all valuable and very helpful for revising and improving our manuscript, as well as the important guiding significance to our researches. We have found a mistake in equation 10 and corrected it. We have studied the valuable comments from you carefully, and tried our best to revise the manuscript. These changes in the revised manuscript have been marked in the track changes version manuscript, as well as the point to point responses have listed as following:

- 1) The reviewer had difficulties to follow some part of the error propagation due to the various introduced coordinate systems denoted as prime without prime and so forth. This made the manuscript very hard to read and one gets easily lost.

Response: We apologize for our unreasonable article structure and denominations to make you confusion. Inspired by your comments, we had removed all denoted primes in coordinate system in revised manuscript. This makes our expression in manuscript more concise and readable. And the three introduced coordinate system can be well distinguished by only using subscripts.

Following your comments, we had carefully rearranged our article structure and reorganized our languages to try to make our article easy to read. We do those changes in revised version:

1. In original manuscript, we established left-hand coordinate systems with right-hand screw rule which is not idiomatic for most readers. Thus, in revised version, we change the coordinate systems to idiomatically right-hand coordinate systems with right-hand screw rule. We hope this change may increase the readability of our manuscript.
2. Section 2 is the main body of this manuscript and we divide it into four parts to make its structure more clearly. We add a brief conclusion of the analytical

process in the end of section 2 (line 275-284). And we add a flow chart to descript our analytical process (Figure 5(a)). In Figure 5(a), the variables and equations in section 2 are all included. We hope that reading section 2 while seeing Figure 5(a) will help readers understand the tedious analytical process.

3. some units or quantitative expressions examples: use the specific angle and distance values to help readers understand the parameters settings in our program (line 282-293); use the specific location error values and resolution values to explain their relationships (line 298-301); use specific rotation angle values to explain the slant of the receiver antennas plane (line 334).
4. Apart from correct the grammar and spelling mistakes you suggested in minor concern, we reread our manuscript to carefully check the spelling, grammar and wording. For example, “traditional meteor radars” is corrected as “classic meteor radars”; “wind retrieving” as “wind retrievals”; “AoA” and “AoAs” are unified as “AoAs”; “clockwise rotation is” as “clockwise rotation satisfies ” et.al.
5. We have found that equation 10 in original version is not correct. We have corrected it and reorganized the relative content in section 2 (line 237-268), figures and code et.al. In corrected version, except there is no “good horizontal resolution area split when baseline is long” , other results are the same.

If you have any confusion, comments or suggestions in revised manuscript, don't hesitate to feedback to us. And we would very pleasure to revise our manuscript and try to make our manuscript better. Thanks for your precious comment.

- 2) Although there are some schematics outlining the coordinate systems the reviewer was not able to follow what actually is shown in Figure 5-7. The reviewer was not able to understand the plots reading the figure caption or the corresponding passage in the text. So please describe the color bars in the text or in the caption what they actually mean.

Response: We apologize for Figure 5-7's poor plots to make you having difficulties in reading the manuscript. Following your suggestion, we carefully replotted original manuscript's Figure 5-7 and the new figures are Figure 6-8 in revised manuscript (because we add an algorithm flow chart and is shown in Figure 5 in new manuscript , the results figures are start from Figure 6). However, due to our rearrange of original manuscript, the new figures do not correspond to original one to one. In original version, we only label the axes with coordinate axes, which is not intuitionistic. And in revised version we label the axes with noun of locality: altitude, east, north and horizontal distance. We hope this change would make readers understand the figures at a glance. In original version, there lack figure captions or corresponding text which makes the figures hard to understand. Therefore, in new version, we add more descriptions in figure captions . Because the deducing process in the section 2 is tedious, we try to provide information as much as possible in figure captions. Moreover, in Figure 6-8 we add subplots titles and colorbar unit (km) to help understand the pictures. For the reason that E_2 related resolution is very smaller comparing with E_1 related and total resolution, we change the colorbar of E_2 related to make this difference visible at a glance, which is not shown well in original one. Thanks very much for your comments and suggestions about our figures. If you have any other confusion, comments or suggestions about revised figures, don't hesitate to feedback to us. And we would very pleasure to carefully revise our manuscript and try to make our pictures more intuitional.

- 3) The reviewer understands that the authors intended to keep things as general as possible, but some units or quantitative expressions are helpful.

Response: Thanks very much for this very precious suggestion. We apologize for our negligence of taking some specific examples to explain some deducing processes or results that are hard to descript or understand. Using some units or

quantitative expressions are a very helpful way to increase readability. Following your suggestion, we add some units or quantitative expressions examples: use the specific angle and distance values to help readers understand the parameters settings in our program (line 282-293); use the specific location error values and resolution values to explain their relationships (line 298-301); use specific rotation angle values to explain the slant of the receiver antennas plane (line 334). If you had any other suggestions about adding some specific quantitative expressions, we would very pleasure to revise our manuscript again.

- 4) In particular, section 2 after line 140 is very hard to read and to follow. This is also partly the case as the Figures are only found at the end of manuscript and one has always to scroll forth and back.

Response: We apologize for our poor structure and presentation in section 2. Following your suggestion, we try our best to rearrange and revise section 2. Section 2 is the main body of this manuscript and we divide it into four parts to make it structure more clearly. We add a brief conclusion of the analytical process in the end of section 2 (line 275-284). We add a flow chart to descript our analytical process (Figure 5(a)). In Figure 5(a), the variables and equations in section 2 are all included. We hope that reading section 2 while seeing Figure 5(a) will help readers understand the tedious analytical process.

- 5) Another important point that should be discussed is that the algebraic errors are just one source that plays a role. The authors should mention in the discussion that there are other error sources as well, originating from the scattering itself or from the experimental set up due to a potential mutual antenna coupling or other obstacles in the surrounding. The later one introduces further biases in the measurements as the angle of arrivals can be significantly altered. Usually, HFSS simulation are required to investigate actually the limits of trustworthiness for the interferometry.

Response: Thanks very much for your suggestion. Inspired by your comments, we mention and discuss the issues of other error sources (line 348-353). The antenna design and site selection are important for meteor radars and HFSS is a powerful tool to study those issues. We only discuss the mathematic error propagation starting from phase difference measuring errors and put emphasis on multistatic configurations. We try to induce things in general, thus the discussion of some specific case of the interferometry maybe beyond the scope of our text. However, if substitute the phase difference measuring errors in our text (set as constant) to values in specific case, our method will still work (line 338-347). There are many detailed works in discuss the interferometry and their AoAs measuring errors in a more specific case, such as (Kang, 2008; Vaudrin et al., Younger and Reid, 2017). These results of AoAs error distribution can be taken into our method to study a more specific case.

- 6) Furthermore, the authors should mention in the discussion that the scattering occurs not really at a singular point. The radio wave is bounced back from at least a few Fresnel zones of several kilometer length along the trajectory, which is actually most relevant for the altitude resolution as the radar signal is scattered from an extended volume (1D) and, thus, probes a volume.

Response: Thanks very much for your suggestions. Following your suggestions, we had carefully thought this issue. The fact that radio wave scattered from a few Fresnel zones around specular point will cause an antenna pair's phase difference deviation from the theoretical expectant value. The theoretical expectant value will resolve a AoAs pointing to specular point. This phase difference deviation is one error source of phase difference measuring errors and is included in phase difference measuring errors ($\delta(\Delta\Psi_1)$ and $\delta(\Delta\Psi_2)$). However, this issue is not clearly point out in our manuscript. Thus, we mention this issue briefly in new version (185-190, 348-350 and Figure 1-2's caption). The details of this issue can be seen in the **RC1 supplement**.

7) It is also worth to mention and discuss the issues of the sampling volume in the context of the trustworthiness of the interferometry. The schematic in Figure 2 provides a nice example of a multistatic geometry resulting in a less good measurement response compared to a monostatic radar of the same measurement volume, although the set up appears to have a multistatic geometry. The measurement response provides a measure of how well a bragg vector can be inverted to still derive reliable wind speeds (u,v,w). Ideally, all three variables can be estimated with similar measurement response, otherwise biases in one of the wind components are not avoidable. The receiver array in Figure 2 defines the sampling volume. Meteors below a certain elevation angle have to be excluded from the analysis due to the mutual antenna coupling or other ground obstacles causing issues in the interferometry.

Response: Very kind of you for your comments. After carefully thinking about your comments, your comments inspired us to add an important discussion about our results (354-363) to mention the issues of sampling volume and measurement response briefly. The measurement response is one of the things that affect the accuracy of Doppler shift. The location error, Doppler shift errors and other issues will determine the accuracy of the wind retrievals. We intend to discuss this in a future work. Following your suggestion, we add two black lines to represent the 30° elevation angle limit in revised figures.

8) Further, it is obvious that the angular diversity of the three links inside the remaining sampling volume is less diverse (all are located in a certain sector relative to the receiver) than a monostatic radar and could systematic bias the wind retrievals. This is the nature of the forward scatter ellipse. As all three forward scatter ellipses have the receiver site in the one of their foci points and the bragg vectors always points towards a point along the distance vector between Rx and Tx. It is further obvious that the longer the total path Rt+Rx becomes the less spatial diversity these vectors have, or with other words – all three links start to see the same geometry as it would

be the case for a monostatic radar. However, building three receiver sites and using one transmitter would increase the sampling volume and if well-distributed compensates some of this sampling effect on the wind analysis (at least partially), but still has a less good measurement response compared to a monostatic system. I suggest that they add in Figure 5-8 a line or shading area indicating the angular limit of the receiver/transmitter array by using a truncation elevation angle of about maybe 30°. The actual limit depends on the array set up.

Response: Thanks very much for your comments. Following your comments, we briefly mention the issue of angular diversity (364-369). However, the impact of angular diversity of Bragg vector on wind retrievals also exceed the topic of our manuscript. We intend to discuss this in a future work. Following your suggestion, we add two black lines to represent the 30° elevation angle limit in revised figures and also mention this issue (line 319-320)

Reference

Ceplecha, Z., Borovička, J., Elford, W. G., ReVelle, D. O., Hawkes, R. L., Porubčan, V., and Šimek, M.: Meteor Phenomena and Bodies, Space Science Reviews, 84, 327-471, 10.1023/A:1005069928850, 1998.

Holdsworth, D. A., Reid, I. M., and Cervera, M. A.: Buckland Park all-sky interferometric meteor radar, Radio Science, 39, <https://doi.org/10.1029/2003RS003014>, 2004.

Hocking, W. K.: Spatial distribution of errors associated with multistatic meteor radar, Earth, Planets and Space, 70, 93, 10.1186/s40623-018-0860-2, 2018.

Kang, C.: Meteor radar signal processing and error analysis, 2008.

Vaudrin, C. V., Palo, S. E., and Chau, J. L.: Complex Plane Specular Meteor Radar Interferometry, Radio Science, 53, 112-128, 10.1002/2017rs006317, 2018.

Younger, J. P., and Reid, I. M.: Interferometer angle-of-arrival determination using precalculated phases, Radio Science, 52, 1058-1066, 10.1002/2017rs006284, 2017.

RC1 Supplement

1. The issue of the radio wave scattered from Fresnel zones

Specular meteor radars (SMR) usually utilize undersense meteor trails. (Ceplecha et al., 1998) discussed radio wave backscatter process with meteors passing though the SMR. In short, for idealized case that ignoring diffusion of meteor trail and assuming that secondary radiative and absorptive effects can be neglected, the return signal received by one antenna can be expressed as:

$$E_{R1}(x_t) = E_0 e^{i(\omega t - 2kR_0)} \int_{-\infty}^{x_t} e^{i(-\pi x^2/2)} dx \quad (1)$$

See figure 1, R_0 is the distance from this antenna 1 to the specular point, or the orthogonal point (t_0 -point hereafter) in other words. $x = \sqrt{\frac{4}{\lambda R_0}} S$ and $k = \frac{2\pi}{\lambda}$. If origin time is when meteor arrives at t_0 point, it will get that $x_t = 2(\lambda R_0)^{-\frac{1}{2}} Vt$ (V is meteor velocity). $\int_{-\infty}^{x_t} e^{i(-\pi x^2/2)} dx$ is a complex Fresnel integral and can be expressed as $C - iS$, where:

$$\begin{aligned} C(x_t) &= \int_{-\infty}^{x_t} \cos(\pi x^2/2) dx \\ S(x_t) &= \int_{-\infty}^{x_t} \sin(\pi x^2/2) dx \end{aligned} \quad (2)$$

Thus, apart from ideal specular reflection signal term “ $e^{i(\omega t - 2kR_0)}$ ”, there is a complex Fresnel modulation term $C - iS$. This modulation will cause amplitude occasion ($\sqrt{C^2 + S^2}$) and phase variation ($\phi_{\text{add}} = \arctan \frac{S}{C}$) in the period a meteor passing through. See figure 2, curve A represent the process based on eq. (1) and curve B, C, D show the effect of including an increasing degree of diffusion of the trail.

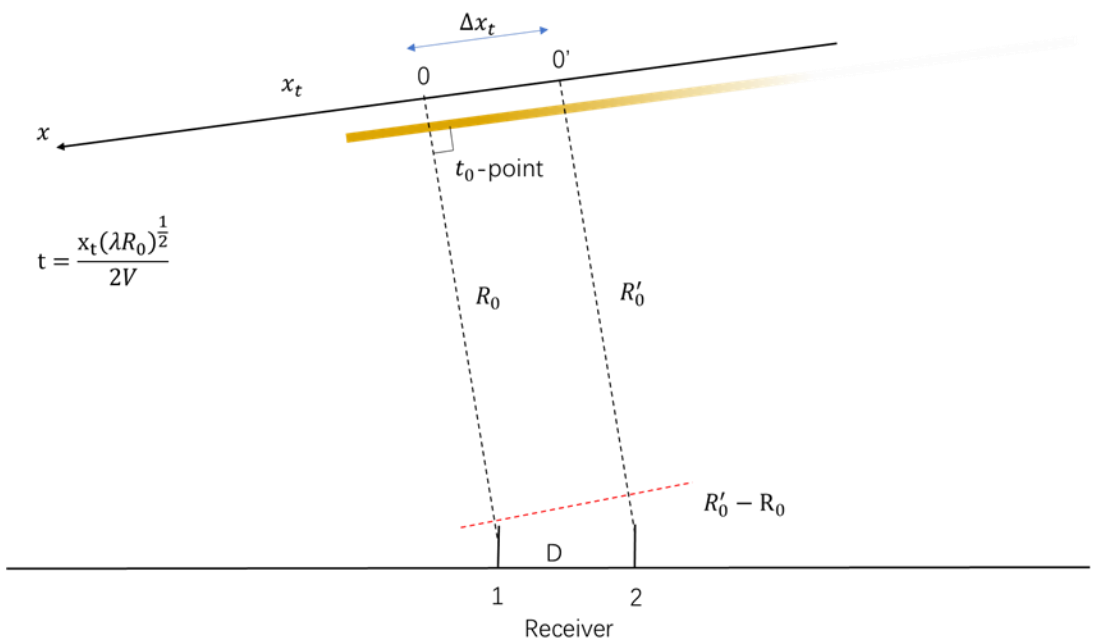


Figure 1

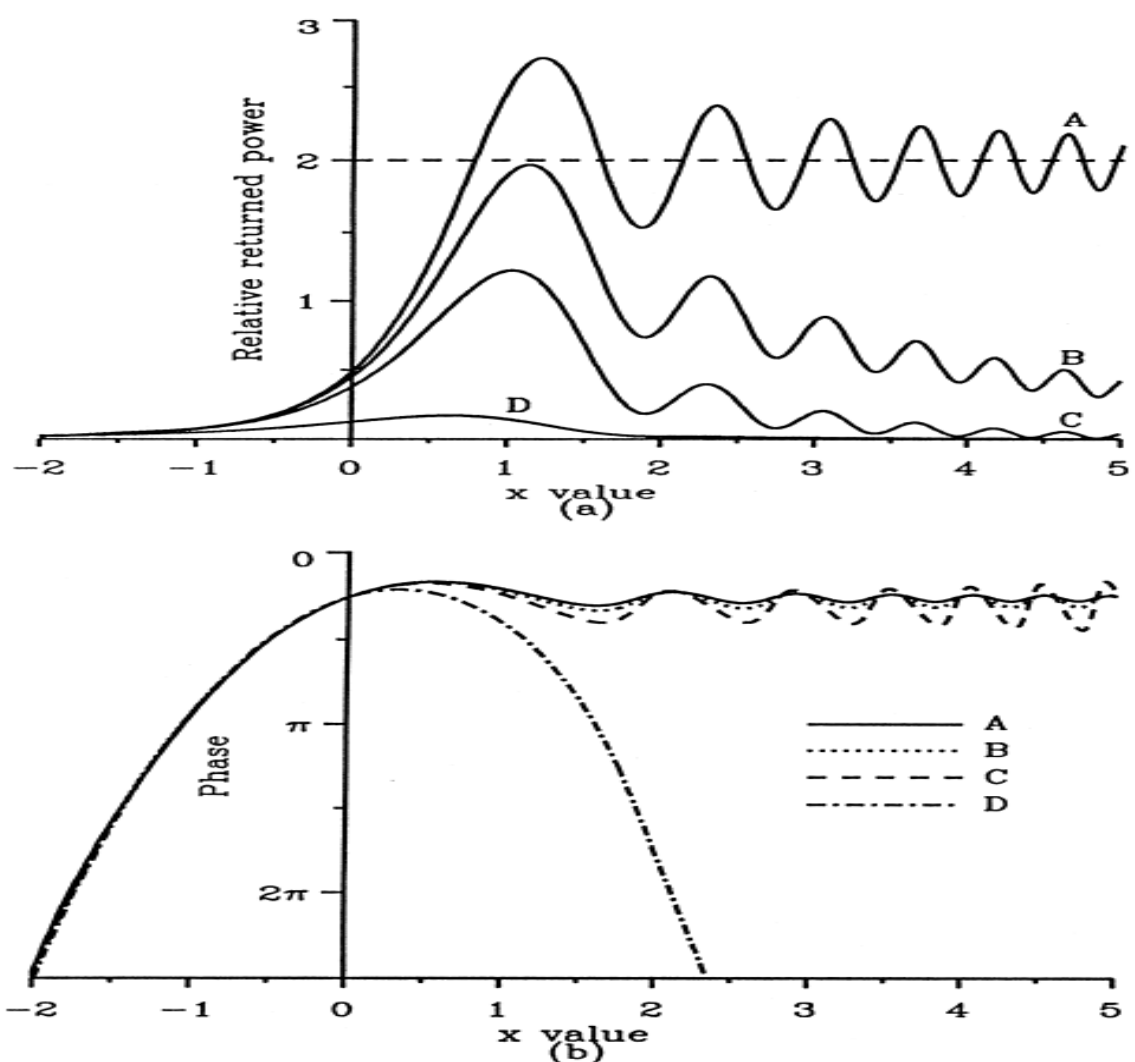


Figure 2(pick from (Ceplecha et al., 1998))

Similarly, the return signal received by antenna 2 is

$$E_{R2}(x_t) = E'_0 e^{i(\omega t - kR_0 - kR'_0)} \int_{-\infty}^{x_t + \Delta x_t} e^{i(-\pi x^2/2)} dx \quad (3)$$

See eq. (1) and (3), the phase difference between two antennas is from second term and third term in right side of the equations. The phase difference caused by second term is $k(R'_0 - R_0)$ which is the theoretical basis of interferometer to obtain AoAs. And this phase difference will solve an AoAs pointing to specular point. However, the third term, which is related to the radio wave scattered from a few Fresnel zone, will cause additional phase difference between two antennas. This additional phase difference is caused by a delay integer length Δx_t between two antennas. For:

$$\Delta x_t = \sqrt{\frac{4}{\lambda R_0}} D \sin \alpha \quad (4)$$

Take a 30MHz meteor radar for example, since $D \sin \alpha \leq 4.5\lambda$ and R_0 is about 100km, Δx_t will not exceed 0.1. The major concern is how big this additional phase difference is. The change rate of the Fresnel modulation phase Φ , i.e. the derivative function of $\arctan(\frac{S}{C})$, will determine the magnitude of this additional phase difference. The Phase changes dramatically in pre- t_0 period and in small concussion after t_0 . The additional phase difference is $\Delta x_t \frac{d\Phi}{dx_t}$ and it's no more than 25 degree around $x_t = -1$ (figure 3). Furthermore, a meteor radar system generally set an amplitude threshold to judge a meteor event and thus IQ analyze is nearly in post- t_0 period which additional phase is very small.

Multistatic meteor radars utilizing the forward scatter is a more general case. The effect of Fresnel zone scatter on measuring errors is nearly the same as monostatic case. See figure 4, t_0 -point is the point where the radio wave path is shortest. Thus t_0 -point is also the specular point where the angle of incidence equals the angle of reflection. T'_x is the symmetry point of T_x about meteor trail (axis-x). For a scatter point x_i alongside the trail, the radio wave propagation path length is the sum of the length from T'_x to x_i and from x_i to an antenna. Therefore t_0 point is the intersection of the trail path and the line from T'_x to an antenna, which represents shortest path length. t_0 point is also specified as the origin of axis-x (or time). For a scatter point x_i which is

S away from t_0 , the radio wave propagation path length can be expressed as:

$$R = \sqrt{R_i^2 + S^2 - 2R_i S \cos(90^\circ + \theta)} + \sqrt{R_s^2 + S^2 - 2R_s S \cos(90^\circ - \theta)} \quad (5)$$

R_i and R_s are specular reflection path length for incident and reflection wave. θ is the incident angle (or reflection angle). Eq. (5) can be expanded to second order because S is very small compared to R_i and R_s . Thus, R can be expressed as:

$$R = R_i + R_s + \left(\cos^2 \theta \left(\frac{1}{R_i} + \frac{1}{R_s} \right) \right) S^2 \quad (6)$$

$R_i + R_s$ correspond to $2R_0$ in monostatic case which represents the shortest path for the radio wave. If substitute $x = \sqrt{\frac{4 \cos^2 \theta (R_i + R_s)}{\lambda R_i R_s}} S$, other process is the same as monostatic case.

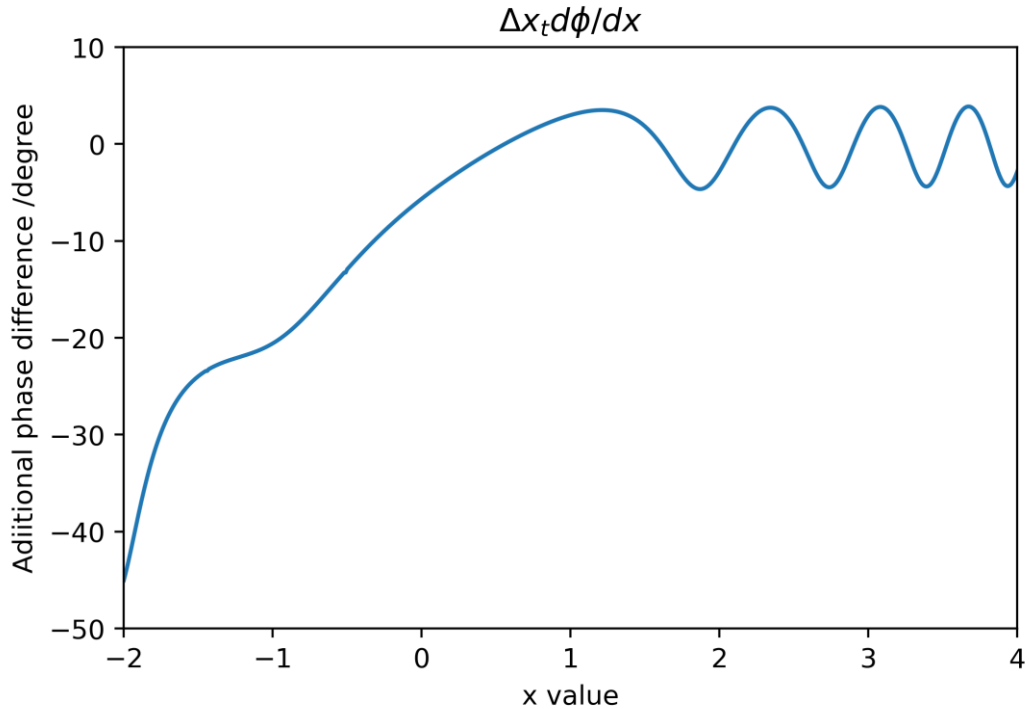


Figure 3

It worth noting that a meteor trail, transmitter and receiver are not always coplanar and a meteor trail and different receiver antenna pairs are not always coplanar too. We only

give a semiquantitative analysis.

Additional phase difference and other measuring errors constitute the phase difference measuring errors ($\delta(\Delta\Psi_1)$ and $\delta(\Delta\Psi_2)$). Different radar system set different $\delta(\Delta\Psi_1)$ and $\delta(\Delta\Psi_2)$. For a receiver in Jones configuration which use at least four pairs of antennas to get AoAs, due to the phase difference measuring errors in those antennas pairs, the system should fit those four measured phase differences to get an expectant AoAs. If the RMS phase difference between the fitted and CCF phase exceeds a preselected threshold (default 20 degree) for any receiver pair the candidate is rejected (Holdsworth et al., 2004). In our program, the default value of $\delta(\Delta\Psi_1)$ and $\delta(\Delta\Psi_2)$ is 35 degree and our error propagation starts from this values. That is to say, the error that caused by the radio wave scatter from a few Fresnel zones of several kilometer length along the trajectory is included in the phase difference measuring errors ($\delta(\Delta\Psi_1)$ and $\delta(\Delta\Psi_2)$) in our analytical method .

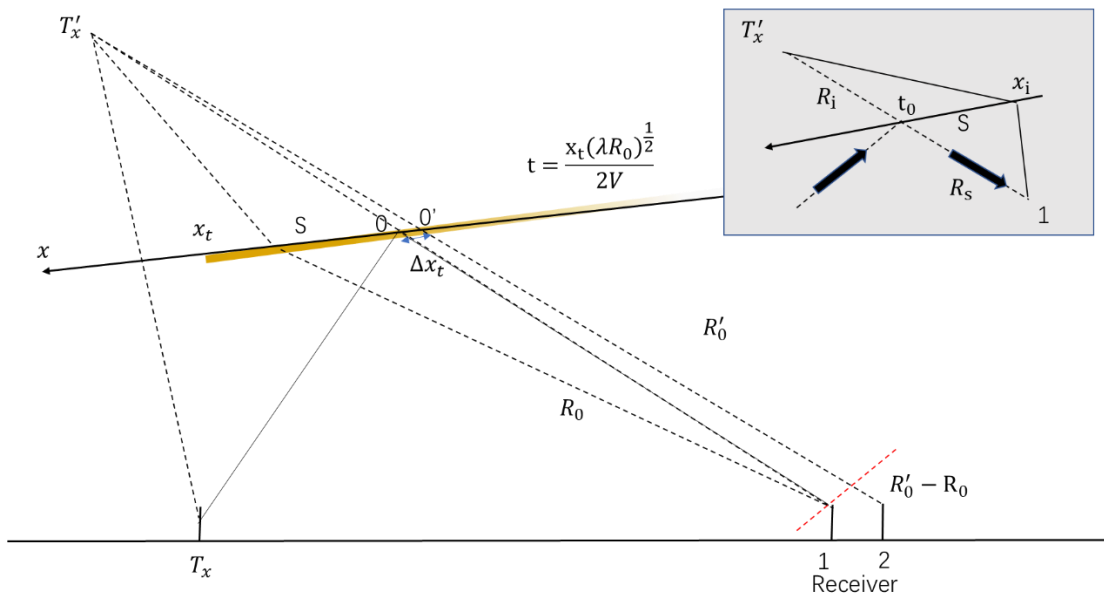


Figure 4

Response to reviewer 2:

Thank your valuable comments and questions concerning our manuscript entitled "Error analyses of a multistatic meteor radar system to obtain a 3-dimensional spatial resolution distribution" [MS no. amt-2020-353]. These comments are all valuable and very helpful for revising and improving our manuscript, as well as the important guiding significance to our researches. We have found a mistake in equation 10 and corrected it. We have studied the valuable comments from you carefully, and tried our best to revise the manuscript. These changes in the revised manuscript have been marked in the track changes version manuscript, as well as the point to point responses have listed as following:

Major comments:

- 1) The manuscript is very difficult to follow, and the English writing needs some improvement.

Response: We apologize for our unreasonable article structure, English writings and denominations to make you have difficulties in reading our article. Following your comments, we carefully rearrange our manuscript and English writing trying to make our manuscript easy to understand. We do those changes in revised version:

1. we had removed all denoted primes in coordinate system in revised manuscript.

This makes our expression in manuscript more concise and readable. And the three introduced coordinate systems can be well distinguished by only using subscripts. Coordinate systems or axes with prime only appear in coordinate rotations.

2. In original manuscript, we established left-hand coordinate systems with right-hand screw rule which is not idiomatic for most readers. Thus, in revised version, we change the coordinate systems to idiomatically right-hand coordinate systems with right-hand screw rule. We hope this change may increase the readability of our manuscript.

3. Section 2 is the main body of this manuscript and we divide it into four parts to make its structure more clearly. We add a brief conclusion of the analytical

process in the end of section 2 (line 275-284). And we add a flow chart to descript our analytical process (Figure 5(a)). In Figure 5(a), the variables and equations in section 2 are all included. We hope that reading section 2 while seeing Figure 5(a) will help readers understand the tedious analytical process.

4. some units or quantitative expressions examples: use the specific angle and distance values to help readers understand the parameters settings in our program (line 282-293); use the specific location error values and resolution values to explain their relationships (line 298-301); use specific rotation angle values to explain the slant of the receiver antennas plane (line 334).
5. Apart from correct the grammar and spelling mistakes you suggested in minor concern, we reread our manuscript to carefully check the spelling, grammar and wording. For example, “traditional meteor radars” is corrected as “classic meteor radars”; “wind retrieving” as “wind retrievals”; “AoA” and “AoAs” are unified as “AoAs”; “clockwise rotation is” as “clockwise rotation satisfies ” et.al.
6. We have found that equation 10 in original version is not correct. We have corrected it and reorganized the relative content in section 2 (line 237-268), figures and code et.al. In corrected version, except there is no “good horizontal resolution area split when baseline is long” , other results are the same.

If you have any confusion, comments or suggestions in revised manuscript, don't hesitate to feedback to us. And we would very pleasure to revise our manuscript and try to make our manuscript better. Thanks for your precious comment.

- 2) Using the term “wind fields” when referring to monostatic systems is not correct. Monostatic meteor radars can be used to retrieve a mean wind vector, but not wind fields. To obtain the latter, one needs to solve for the gradients. And $[du/dy]$, $[dv/dx]$ can only be estimated when at least a bi-static configuration is taken into account. In connection with this issue, please re-write lines 35-50. Even with a good azimuthal sampling, the shearing term (besides the vorticity) cannot be estimated using a monostatic system. Only $[du/dx]$, $[dv/dy]$ can be estimated from monostatic measurements, but not $[du/dy]$, $[dv/dx]$. The latter means that not only the vorticity

cannot be obtained, but neither the shearing term. Besides, there is no need to have a measure of the vertical wind in order to estimate the horizontal divergence.

Response: Thanks for your comments very much. We apologize for our inaccurate wording in original manuscript. Although monostatic using VAD or VVP could obtain $\frac{du}{dx}, \frac{dv}{dy}$ in certain situations, all four gradient components can not be obtained. Thus, “wind field” is not accurate for monostatic meteor radars. Following your comments, we substitute “wind field” in line 34 to “wind” for accuracy.

In original manuscript in line 35-50, we are actually discussing the case of Doppler weather radars used in troposphere measurement. We apologize for our straying from the point which had mislead you. In troposphere, atmospheric activities are strong in vertical, thus the vertical wind component projected to radial sight of the radar can not be neglected (in MLT however, the vertical wind component can be ignored). Moreover, those weather radars need to measure vertical wind components to study precipitation process of the troposphere. To obtain horizontal wind information, the vertical wind component should be removed from radial Doppler shift at first. A simple way to resolve it is using a vertical beam to detect the vertical wind. In the sampling volume, the vertical wind are assumed as the same. However, inspired by your comments, we reconsider the paragraph in line 35-50 and realize that the discussion of weather radar in this text is not suitable and will mislead the readers. Thus, we rewrite lines 35-50 only discuss the case of classic meteor radar. This makes our text more concise and keep to the point. Thanks very much for your comments.

Finally, after carefully recheck the issue of gradient components retrieving, we find that the shearing term can be obtained. Although “ $\frac{du}{dy}$ ” and “ $\frac{dv}{dx}$ ” can not be solved individually, their sum value (i.e. shearing term) can be obtained (Browning and Wexler, 1968). Or in other words, their subtract value (i.e. vorticity) can’t be

known thus can't obtain " $\frac{du}{dy}$ " and " $\frac{dv}{dx}$ " individually. Details can be seen in **RC2 supplement**.

- 3) Instead of referring to a previous work, it would better if the authors included a simple sketch in order to understand how equation (1) is obtained.

Response: Thanks for your suggestions very much. Following your suggestion, the figure 4(a) is used as a sketch to help readers understand eq.(1) and we simply explain how to obtain this equations (line 124).

- 4) Furthermore, the algebraic deductions of the error propagation matrixes presented in the appendixes should be treated with more care. For example, in appendix A.2, it would be helpful to have clearly indicated in its corresponding figure the angles γ_1 , γ_2 , θ , and φ . This would help to understand, e.g., how equations A2.3 and A2.4 are obtained.

Response: Very kind of you for your suggestions. We apologize for our carelessness in treating with appendix. Following your suggestions, we carefully revise the appendix.

Some of the grammar and wordings changes are as follows:

1. In appendix A.1 in line 461 and 463, we delete Z' which will cause the misleading and substitute it with "the new coordinate".
2. In appendix A.1 in line 471, "For any two coordinate systems XYZ and $X'Y'Z'$ ", we add with co-origin for more accurate.
3. In appendix A.2 in line 479, "The AoAs is determined by two phase difference $\Delta\Psi_1$ and $\Delta\Psi_2$. Taking one antenna array as an example and Assuming " is deleted and substitute it with "In the plane wave approximation,"
4. In original manuscript, "using Taylor expression of ..." is not concise and accurate. In revised manuscript, we substitute it with "Expand XXX in eq.X to first order, ..."
5. In original manuscript, too many "We ..." are used. In revised manuscript, we change most of them to passive voice.

Figure A.1 and A.2 are also revised following your suggestions. Figure A.1's rotation marks aren't conformed to three-dimensional perspective and will cause misleading in original version. In new version, we replot it and it can show the relationship of cover between objects. We hope this may help readers. Figure A.2 in new version adds θ and ϕ to help readers understand the deducing of equations.

- 5) In the case of appendix A.1, please modify its corresponding figure. Since the authors use lefthanded coordinate systems but follow the right-hand corkscrew rule, figure A.1 in its present form does not help to understand appendix A.1.

Response: In original manuscript, we established left-hand coordinate systems which is not idiomatical for most readers. Thus, in revised version, we change the coordinate systems to idiomatically right-hand coordinate systems. We hope this change may increase the readability of our manuscript. Correspondingly, we modify figure A.1 in righthanded coordinate systems and follow the right-hand corkscrew rule.

- 6) Figures 5 to 8 contain the most important results of this work but they are poorly described and barely discussed. Besides, some of the statements based on these figures are not evident, at least for this reviewer. For example, what is stated in lines 225-226 is not obvious for the eyes of this reviewer.

Response: We apologize for Figure 5-7's poor plots to make you having difficulties in reading the manuscript. Following your suggestion, we carefully replotted original manuscript's Figure 5-7 and the new figures are Figure 6-8 in revised manuscript (because we add an algorithm flow chart and is shown in Figure 5 in new manuscript, the results figures are start from Figure 6). However, due to our rearrange of original manuscript, the new figures do not correspond to original one to one. In original version, we only label the axes with denoted coordinate axes with prime (X'_0, Y'_0, Z'_0), which is not intuitionistic. And in revised version we label the axes with noun of locality: altitude, east, north and horizontal distance. We hope this change would understand figures at a glance. In original version, there lack

figure captions or corresponding text which makes the figures hard to understand. Therefore, in new version, we add more descriptions in figure captions not only in Figure 6-8, but also Figure 1-5's Schematic diagram or flow chart. We try to provide information as much as possible in figure captions. Moreover, in Figure 6-8 we add subplots titles and colorbar unit (km) to help understand the pictures.

For the reason that E_2 related resolution is very smaller comparing with E_1 related and total resolution, we change the colorbar of E_2 related to make this difference visible at a glance, which is not shown well in original one. Thanks very much for your comments and suggestions about our figures. If you have any other confusion, comments or suggestions about revised figures, don't hesitate to feedback to us. And we would very pleasure to carefully revise our manuscript and try to make our pictures more intuitional.

- 7) This reviewer understands that the authors' objective is to analyse the errors that result from the multistatic configuration. However, the existence of other errors should be mentioned in the paper and a brief discussion on how they compare to the errors here analysed should be included. For example, it is known that the echoes do not originate on a single point in space. So, how large would it be the impact of this on the vertical resolution? Or can it be neglected?

Response: Thanks very much for your suggestion. Inspired by your comments, we mention and discuss the issues of other error sources (line 348-353). The antenna design and site selection are important for meteor radars and HFSS is a powerful tool to study those issues. We only discuss the mathematic error propagation starting from phase difference measuring errors and put emphasis on multistatic configurations. We try to induce things in general, thus the discussion of some specific case of the interferometry maybe beyond the scope of our text. However, if substitute the phase difference measuring errors in our text (set as constant) to values in specific case, our method will still work (line 338-347). There are many detailed works in discuss the interferometry and their AoAs measuring errors in a more specific case, such as (Kang, 2008; Vaudrin et al., Younger and Reid, 2017). These results of AoAs error distribution can be taken into our method to study a more specific case.

Following your suggestions, we had carefully thought the issue of the radio wave scattered from Fresnel zones. The fact that radio wave scattered from a few Fresnel zones around specular point will cause an antenna pair's phase difference deviation from an ideal expectant value. The ideal expectant value will resolve a AoAs pointing to specular point. This phase difference deviation is one error source of phase difference measuring errors. Thus the impact of Fresnel scatter on measuring errors is included in phase difference measuring errors ($\delta(\Delta\Psi_1)$ and $\delta(\Delta\Psi_2)$). However, this issue is not clearly point out in our manuscript. Thus, we mention this issue briefly in new version (185-190, 348-350 and Figure 1-2's caption). The details of this issue can be seen in the **RC2 supplement**.

- 8) Maybe it is out of the scope of this work, but it would be helpful if some data were considered in the study. For example, what does really mean having a spatial resolution of let us say, 2-3 km? How would this impact on winds and horizontal gradients estimates? Have the authors made any rough estimation of this? It would be very useful for the readers if some information on this was included in the manuscript.

Response: Very kind of you for your suggestions. After carefully thinking your suggestions, your suggestions inspired us to add an important discussion about our results to briefly mention the issues of wind retrieving (line 354-369). Also, we add examples to explain the meaning of the spatial resolution, to use specific location error values and resolution values to explain their relationships (line 298-301).

The location error, Doppler shift errors and other issues will determine the accuracy of the wind retrievals. We intend to discuss this in a future work. The location error of the meteor trail's specular point, or the spatial resolution in other words, is discussed in this manuscript. Our manuscript is about 8500 word and includes the tedious analytical process with many equations. we think it would be better for our manuscript concentrate on the discussion of spatial resolutions. We will try our best to make up real data and wind retrieving discussion as soon as possible in the next.

Minor comments:

- 1) Line 30: please include more references here. Studies from other scientific institutions, e.g., Leipzig University and the Leibniz-IAP (Germany), which have long traditions on studies based on meteor radar measurements should be included.

Response: Thanks for your suggestion. We apologize for our omissions of citing Leipzig University and the Leibniz-IAP (Germany) in line 30. Leipzig University and the Leibniz-IAP have long traditions on studying meteor radars and done many excellent works about multistatic radars in recent years. Therefore, following your suggestion we add “(Jacobi et al., 2008; Stober et al., 2013)” in line 31 in revised version.

- 2) Line 32: please change “... same height range be processed...” to “... same height range are processed...”

Response: corrected.

- 3) Line 48: “Even by releasing...”. I think the authors meant “relaxing”.

Response: corrected. Thanks for pointing out this typo.

- 4) Lines 53 and 59: it is MMARIA, not MMARA. Please change that.

Response: corrected. Thanks for pointing out this typo.

- 5) Line 62: it should be “... Chau et al. used two adjacent...” and not “Stober et al.”

Response: corrected. Thanks for pointing out this typo.

- 6) Lines 65-66, what do the authors mean with “meteor radar data processing method”?

Response: Thanks for your comment. Following your comment, we change “meteor radar data processing method” to “coded continuous wave meteor radar”.

- 7) Lines 68: please change “... of received signals, we can determine...” to “... of received signals, one can determine...”. The same change should be applied in lines 69 and 71.

Response: corrected. Thanks for your suggestion. We also do same changes in line 151,153,155. We change the sentences using “we ...” to passive voice, too.

8) Line 101: “to the cosine of the zenith angle”

Response: corrected. Thanks for your suggestion.

9) Line 199: “and is president in supplement...”. Do the authors mean “and is presented in the supplement”?

Response: yes. Thanks for pointing out this typo. We corrected “president” to “presented”.

10) Please make figures 5 to 8 self-contained. One should be able to understand the main message of a figure without reading the caption.

Response: corrected. We add titles for Figures and the labels of axes are changed to “Altitude”, “East”, “West” and “Horizontal distance” to make figures visualized.

The figure 8 in new version is a 3D contourf plot for intuitional.

Reference:

Browning, K. A., and Wexler, R.: The Determination of Kinematic Properties of a Wind Field Using Doppler Radar, *Journal of Applied Meteorology*, 7, 105-113, 10.1175/1520-0450(1968)007<0105:Tdokpo>2.0.Co;2, 1968.

Browning, K. A., and Wexler, R.: The Determination of Kinematic Properties of a Wind Field Using Doppler Radar, *Journal of Applied Meteorology*, 7, 105-113, 10.1175/1520-0450(1968)007<0105:Tdokpo>2.0.Co;2, 1968.

Jacobi, C., Hoffmann, P., and Kärschner, D.: Trends in MLT region winds and planetary waves, Collm (52°N, 15°E), *Annales Geophysicae (ANGEOP)*, 2008.

Stober, G., Sommer, S., Rapp, M., and Latteck, R.: Investigation of gravity waves using horizontally resolved radial velocity measurements, *Atmos. Meas. Tech.*, 6, 2893-2905, 10.5194/amt-6-2893-2013, 2013.

Hocking, W. K.: Spatial distribution of errors associated with multistatic meteor radar, *Earth, Planets and Space*, 70, 93, 10.1186/s40623-018-0860-2, 2018.

Kang, C.: Meteor radar signal processing and error analysis, 2008.

Vaudrin, C. V., Palo, S. E., and Chau, J. L.: Complex Plane Specular Meteor Radar Interferometry, *Radio Science*, 53, 112-128, 10.1002/2017rs006317, 2018.

Younger, J. P., and Reid, I. M.: Interferometer angle-of-arrival determination using precalculated phases, *Radio Science*, 52, 1058-1066, 10.1002/2017rs006284, 2017.

RC2 Supplement

1. The issue about how to obtain shearing term for a monostatic radar

In MLT region, we assume that the horizontal wind field in a certain altitude H can be expressed as:

$$u(x, y) = u_0 + \frac{\partial u}{\partial x} x + \frac{\partial u}{\partial y} y \quad (1)$$

$$v(x, y) = v_0 + \frac{\partial v}{\partial x} x + \frac{\partial v}{\partial y} y \quad (2)$$

u_0 and v_0 are mean wind component. Without loss of generality, the origin of coordinate-xy can be set in right above the radar. The vertical wind can be ignored.

A radial Doppler shift correspond to a radial wind velocity, denoted as $V_R(\theta, \phi)$. θ, ϕ are zenith and azimuth angle of a radial direction. The unit vector in radial, denoted as \vec{n}_R is:

$$\vec{n}_R = (\sin\theta\cos\phi, \sin\theta\sin\phi, \cos\theta) \quad (3)$$

The wind field is projected to the radial direction and is measured by radars as V_R :

$$V_R(\theta, \phi) = \vec{n}_R(\theta, \phi) \cdot \vec{V}(x, y) \quad (4)$$

$$\vec{V}(x, y) = (u(x, y), v(x, y), 0) \quad (5)$$

$$(x, y) = (H\tan\theta\cos\phi, H\tan\theta\sin\phi) \quad (6)$$

simultaneous equation (1)-(6):

$$\begin{aligned} V_R(\theta, \phi) = & \sin\theta\cos\phi u_0 + \sin\theta\sin\phi v_0 + H\tan\theta\cos\phi\sin\theta\cos\phi \frac{\partial u}{\partial x} + \\ & H\tan\theta\sin\phi\sin\theta\cos\phi \frac{\partial u}{\partial y} + H\tan\theta\cos\phi\sin\theta\sin\phi \frac{\partial v}{\partial x} + H\tan\theta\sin\phi\sin\theta\sin\phi \frac{\partial v}{\partial y} \end{aligned} \quad (7)$$

In equation (7), there are 6 variables need to be solved (mean wind and four gradient components: $u_0, v_0, \frac{\partial u}{\partial x}, \frac{\partial u}{\partial y}, \frac{\partial v}{\partial x}, \frac{\partial v}{\partial y}$). However, the coefficients ahead $\frac{\partial v}{\partial x}$ and $\frac{\partial u}{\partial y}$ are the same.

This means that at most 5 variables can be obtained. By combing four and five term in right of equation (7), we can obtain:

$$\begin{aligned} V_R(\theta, \phi) = & \sin\theta\cos\phi u_0 + \sin\theta\sin\phi v_0 + H\tan\theta\cos\phi\sin\theta\cos\phi \frac{\partial u}{\partial x} + \\ & H\tan\theta\sin\phi\sin\theta\sin\phi \frac{\partial v}{\partial y} + H\tan\theta\sin\phi\sin\theta\cos\phi \left(\frac{\partial u}{\partial y} + \frac{\partial v}{\partial x} \right) \end{aligned} \quad (8)$$

In equation (8), the five coefficient are mutually different thus five variables can be solved.

They are mean wind u_0, v_0 , two gradient components $\frac{\partial u}{\partial x}, \frac{\partial u}{\partial y}$ and shearing term $(\frac{\partial u}{\partial y} + \frac{\partial v}{\partial x})$.

2. The issue of the radio wave scattered from Fresnel zones

Specular meteor radars (SMR) usually utilize undersense meteor trails. (Ceplecha et al., 1998) discussed radio wave backscatter process with meteors passing though the SMR. In short, for idealized case that ignoring diffusion of meteor trail and assuming that secondary radiative and absorptive effects can be neglected, the return signal received by one antenna can be expressed as:

$$E_{R1}(x_t) = E_0 e^{i(\omega t - 2kR_0)} \int_{-\infty}^{x_t} e^{i(-\pi x^2/2)} dx \quad (1)$$

See figure 1, R_0 is the distance from this antenna 1 to the specular point, or the orthogonal point (t_0 -point hereafter) in other words. $x = \sqrt{\frac{4}{\lambda R_0}} S$ and $k = \frac{2\pi}{\lambda}$. If origin time is when meteor arrives at t_0 point, it will get that $x_t = 2(\lambda R_0)^{-\frac{1}{2}} V t$ (V is meteor velocity). $\int_{-\infty}^{x_t} e^{i(-\pi x^2/2)} dx$ is a complex Fresnel integral and can be expressed as $C - iS$, where:

$$C(x_t) = \int_{-\infty}^{x_t} \cos(\pi x^2/2) dx$$

$$S(x_t) = \int_{-\infty}^{x_t} \sin(\pi x^2/2) dx \quad (2)$$

Thus, apart from ideal specular reflection signal term “ $e^{i(\omega t - 2kR_0)}$ ”, there is a complex Fresnel modulation term $C - iS$. This modulation will cause amplitude occasion ($\sqrt{C^2 + S^2}$) and phase variation ($\phi_{\text{add}} = \arctan \frac{S}{C}$) in the period a meteor passing through. See figure 2, curve A represent the process based on eq. (1) and curve B, C, D show the effect of including an increasing degree of diffusion of the trail.

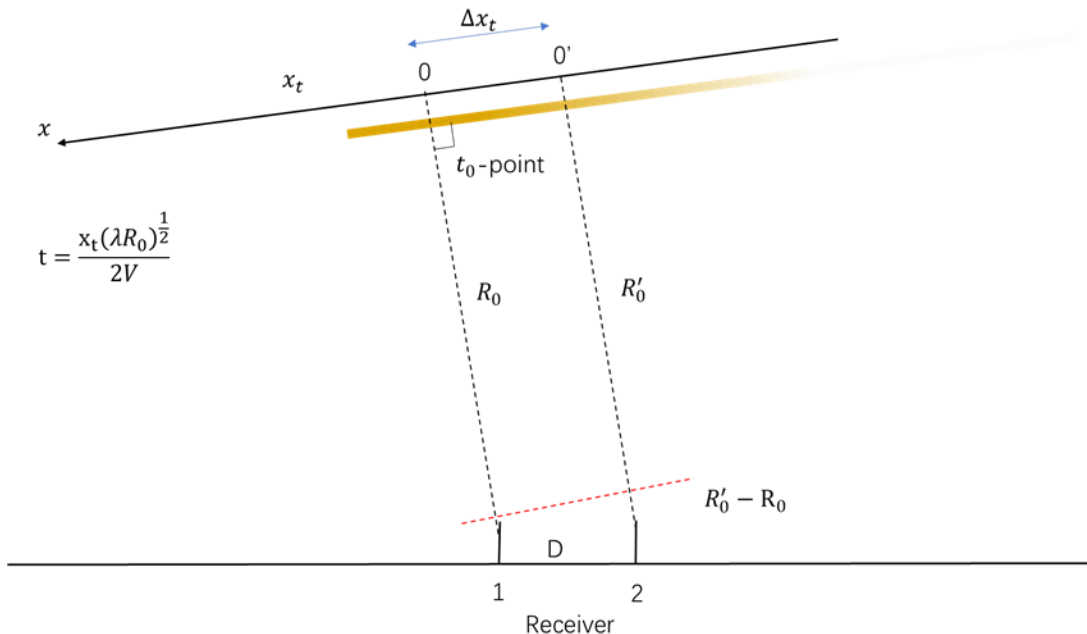


Figure 1

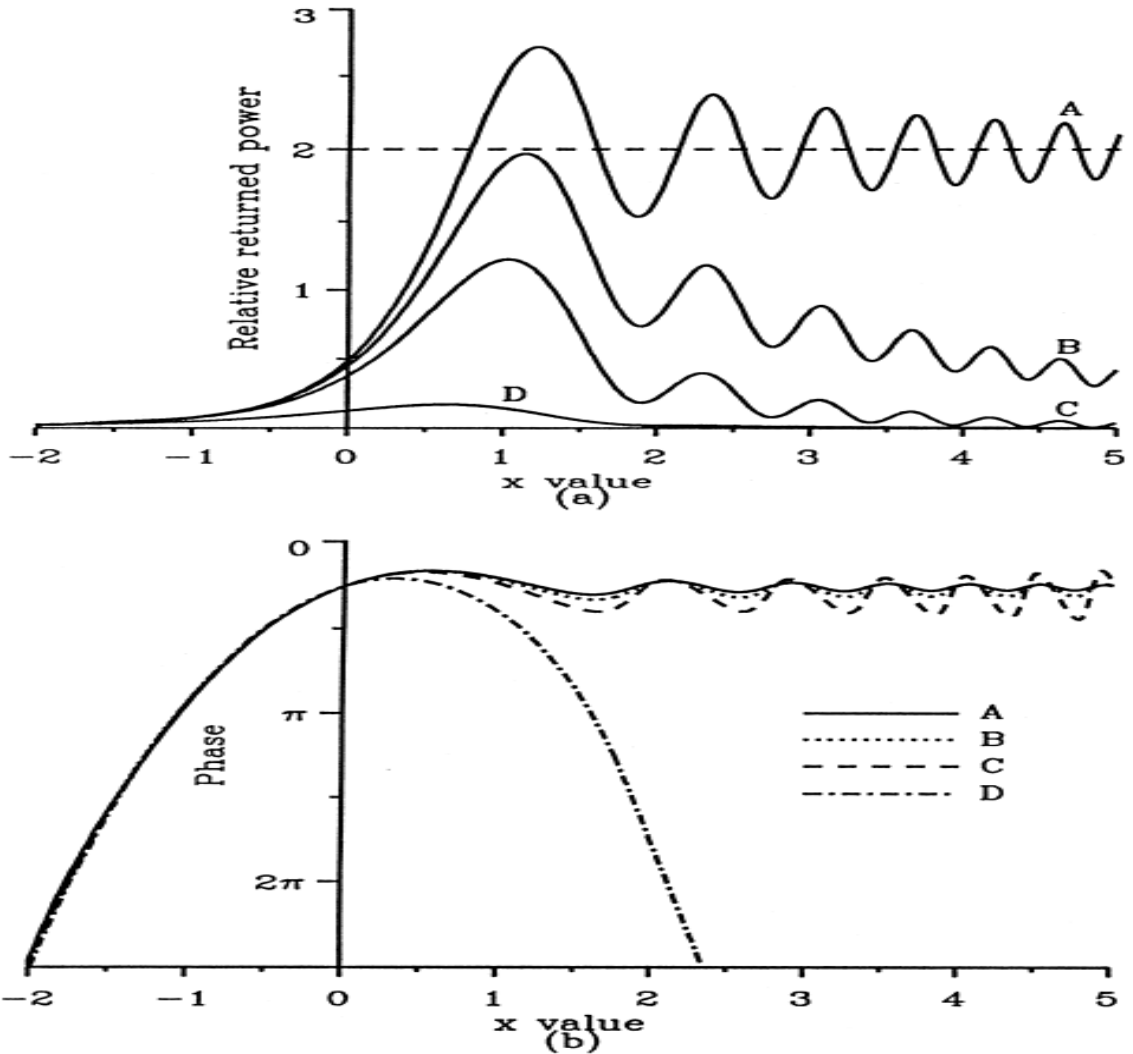


Figure 2(pick from (Ceplecha et al., 1998))

Similarly, the return signal received by antenna 2 is

$$E_{R2}(x_t) = E'_0 e^{i(\omega t - kR_0 - kR'_0)} \int_{-\infty}^{x_t + \Delta x_t} e^{i(-\pi x^2/2)} dx \quad (3)$$

See eq. (1) and (3), the phase difference between two antennas is from second term and third term in right side of the equations. The phase difference caused by second term is $k(R'_0 - R_0)$ which is the theoretical basis of interferometer to obtain AoAs. And this phase difference will solve an AoAs pointing to specular point. However, the third term, which is related to the radio wave scattered from a few Fresnel zone, will cause additional phase difference between two antennas. This additional phase difference is caused by a delay integer length Δx_t between two antennas. For:

$$\Delta x_t = \sqrt{\frac{4}{\lambda R_0}} D \sin \alpha \quad (4)$$

Take a 30MHz meteor radar for example, since $D \sin \alpha \leq 4.5\lambda$ and R_0 is about 100km, Δx_t will not exceed 0.1. The major concern is how big this additional phase difference is. The change rate of the Fresnel modulation phase Φ , i.e. the derivative function of $\arctan(\frac{S}{C})$, will determine the magnitude of this additional phase difference. The Phase changes dramatically in pre- t_0 period and in small concussion after t_0 . The additional phase difference is $\Delta x_t \frac{d\Phi}{dx_t}$ and it's no more than 25 degree around $x_t = -1$ (figure 3). Furthermore, a meteor radar system generally set an amplitude threshold to judge a meteor event and thus IQ analyze is nearly in post- t_0 period which additional phase is very small.

Multistatic meteor radars utilizing the forward scatter is a more general case. The effect of Fresnel zone scatter on measuring errors is nearly the same as monostatic case. See figure 4, t_0 -point is the point where the radio wave path is shortest. Thus t_0 -point is also the specular point where the angle of incidence equals the angle of reflection. T'_x is the symmetry point of T_x about meteor trail (axis-x). For a scatter point x_i alongside the trail, the radio wave propagation path length is the sum of the length from T'_x to x_i and from x_i to an antenna. Therefore t_0 point is the intersection of the trail path and the line from T'_x to an antenna, which represents shortest path length. t_0 point is also specified as the origin of axis-x (or time). For a scatter point x_i which is S away from t_0 , the radio wave propagation path length can be expressed as:

$$R = \sqrt{R_i^2 + S^2 - 2R_i S \cos(90^\circ + \theta)} + \sqrt{R_s^2 + S^2 - 2R_s S \cos(90^\circ - \theta)} \quad (5)$$

R_i and R_s are specular reflection path length for incident and reflection wave. θ is the incident angle (or reflection angle). Eq. (5) can be expanded to second order because S is very small compared to R_i and R_s . Thus, R can be expressed as:

$$R = R_i + R_s + \left(\cos^2 \theta \left(\frac{1}{R_i} + \frac{1}{R_s} \right) \right) S^2 \quad (6)$$

$R_i + R_s$ correspond to $2R_0$ in monostatic case which represents the shortest path for the radio wave. If substitute $x = \sqrt{\frac{4 \cos^2 \theta (R_i + R_s)}{\lambda R_i R_s}} S$, other process is the same as monostatic case.

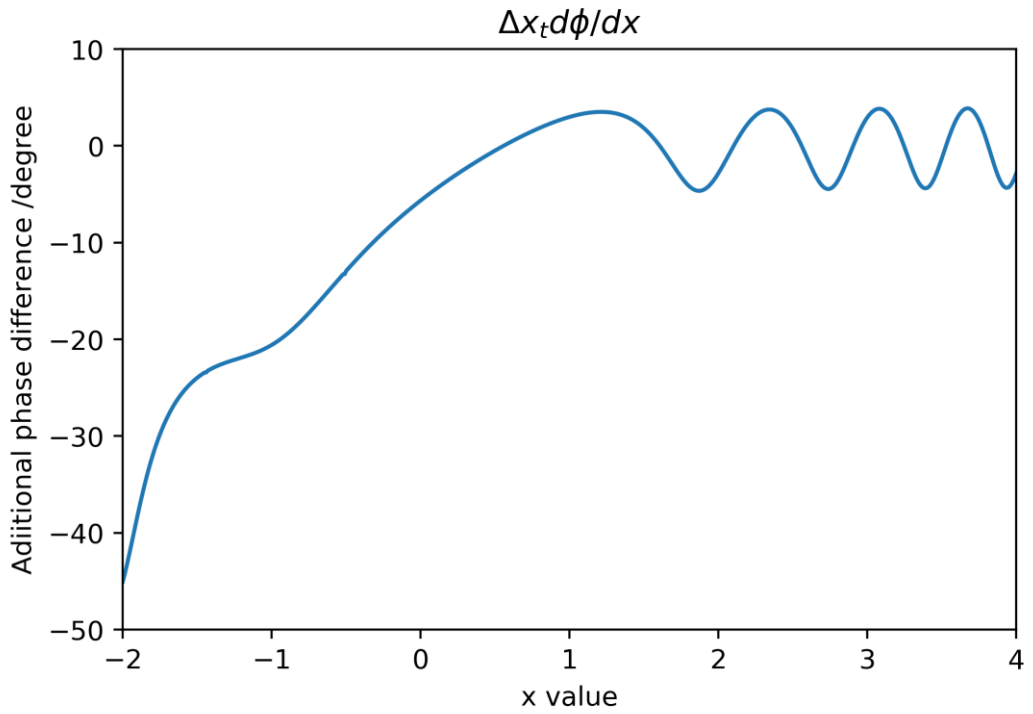


Figure 3

It is worth noting that a meteor trail, transmitter and receiver are not always coplanar and a meteor trail and different receiver antenna pairs are not always coplanar too. We only give a semiquantitative analysis.

Additional phase difference and other measuring errors constitute the phase difference measuring errors ($\delta(\Delta\Psi_1)$ and $\delta(\Delta\Psi_2)$). Different radar system set different $\delta(\Delta\Psi_1)$ and $\delta(\Delta\Psi_2)$. For a receiver in Jones configuration which use at least four pairs of antennas to get AoAs, due to the phase difference measuring errors in those antennas pairs, the system should fit those four measured phase differences to get an expectant AoAs. If the RMS phase difference between the fitted and CCF phase exceeds a preselected threshold (default 20 degree) for any receiver pair the candidate is rejected (Holdsworth et al., 2004). In our program, the default value of $\delta(\Delta\Psi_1)$ and $\delta(\Delta\Psi_2)$ is 35 degree and our error propagation starts from this values. That is to say, the error that caused by the radio wave scatter from a few Fresnel zones of several kilometer length along the trajectory is included in the phase difference measuring errors

$(\delta(\Delta\Psi_1)$ and $\delta(\Delta\Psi_2))$ in our analytical method .

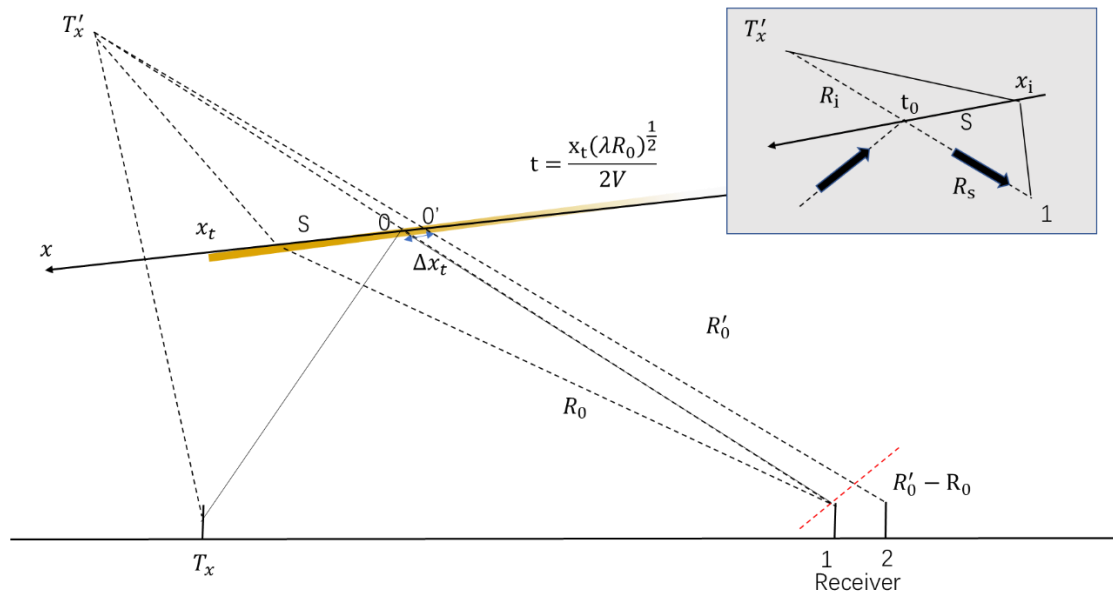


Figure 4

Error analyses of a multistatic meteor radar system to obtain a 3-dimensional spatial resolution distribution

Wei Zhong¹, Xianghui Xue^{1,2,3}, Wen Yi^{1,2}, Iain M. Reid^{4,5} Tingdi Chen^{1,2,3}, Xiankang Dou^{1,6}

¹CAS Key Laboratory of Geospace Environment, Department of Geophysics and Planetary Sciences, University of Science and Technology of China, Hefei, China

²Mengcheng National Geophysical Observatory, School of Earth and Space Sciences, University of Science and Technology of China, Hefei, China

³CAS Center for Excellence in Comparative Planetology, Hefei, China

⁴ATRAD Pty Ltd., Thebarton, South Australia, Australia

⁵School of Physical Sciences, University of Adelaide, Adelaide, South Australia, Australia

⁶Wuhan University, Wuhan, China

Correspondence to: Xianghui Xue (xuexh@ustc.edu.cn)

Abstract: In recent years, the concept of multistatic meteor radar systems has attracted the attention of the atmospheric radar community, focusing on the mesosphere and lower thermosphere (MLT). Recently, there have been some notable experiments using multistatic meteor radar systems. Good spatial resolution is vital for meteor radars because nearly all parameter inversion processes rely on the accurate location of the meteor trail reflecting points the meteor trail specular point. It is timely then for a careful discussion focussed on the error distribution of multistatic meteor radar systems. In this study, we discuss the measurement errors that affect the spatial resolution and obtain the spatial resolution distribution in 3-dimensional space for the first time. The spatial resolution distribution can both help design a multistatic meteor radar system and improve the performance of existing radar systems. Moreover, the spatial resolution distribution allows the accuracy of retrieved parameters such as the wind fields to be determined.

1 Introduction

The mesosphere and lower thermosphere (MLT) is a transition region from the neutral to the partially ionized atmosphere. It is dominated by the effects of atmospheric waves, including planetary waves, tides and gravity waves. It is also a relatively poorly sampled part of the Earth's atmosphere by ground-based instruments. One widely used approach to sample this region is the meteor radar technique. The ablation of incoming meteors in the MLT region, i.e., $\sim 80 - 110$ km, creates layers of metal atoms, which can be observed from the ground by photometry or lidar (Jia et al., 2016; Xue et al., 2013). During meteor ablation, the trails caused by small meteor particles provide a strong atmospheric tracer within the MLT region that can be continuously detected by meteor radar regardless of weather conditions. Consequently, the meteor radar technique has been a powerful tool for studying MLT for decades (Hocking et al., 2001; Holdsworth et al., 2004; Jacobi et al., 2008; Stober et al., 2013; Yi et al., 2018). Most modern meteor radars are monostatic and this has two main limitations in retrieving the complete

wind fields. Firstly, limited meteor rates and relatively low measurement accuracies necessitate that all measurements in the same height range are processed to calculate a “mean” wind. Secondly, traditional classic monostatic radars retrieve wind fields based on the assumption of a homogenous wind fields in horizontal direction and a zero wind in the vertical direction.

35 The latter conditions can be partly relaxed if the count rates are high and the detections are distributed through a representative range of azimuths. If this is the case, a version of a Velocity Azimuth Display (VAD) analysis as first applied to scanning weather radars for longer period motions can be applied by expanding the zonal and meridional winds using a truncated Taylor expansion (Browning and Wexler, 1968). This is because each valid meteor detection yields a radial velocity in a particular look direction of the radar. The radar is effectively a multi-beam Doppler radar where the “beams” are determined by the 40 meteor detections. If there are enough suitably distributed detections in azimuth in a given observing period, the Taylor expansion approach using cartesian coordinates yields the mean zonal and meridional wind components (u_0, v_0), the horizontal divergence $(\frac{\partial u}{\partial x} + \frac{\partial v}{\partial y})$, the stretching $(\frac{\partial u}{\partial x} - \frac{\partial v}{\partial y})$ and the shearing $(\frac{\partial u}{\partial y} + \frac{\partial v}{\partial x})$ deformations of the wind fields from an analysis of the radial velocities. If a measure of the vertical wind is available, then the horizontal divergence $(\frac{\partial u}{\partial x} + \frac{\partial v}{\partial y})$ can also be obtained (assuming a uniform vertical wind over the observing volume). Generally, meteor radars do not provide a reliable 45 measure of the vertical wind 45 component. In addition, because the radar can only retrieve the wind projection in the radial direction as measured from the radar, the vorticity $(\frac{\partial v}{\partial x} - \frac{\partial u}{\partial y})$ of the wind field is not available. However, because the radar can only retrieve the wind projection in the radial direction as measured from the radar, the vorticity $(\frac{\partial v}{\partial x} - \frac{\partial u}{\partial y})$ of the wind fields is not available. This is common to all monostatic radar systems and a discussion of measurable parameters in the context of multiple fixed beam upper atmosphere Doppler radars is given by (Reid, 1987). Even by relaxing the assumption of a 50 homogeneous wind fields and using the more advanced Volume Velocity Processing (VVP) (Philippe and Corbin, 1979) to retrieve the wind fields, the horizontal gradients of the wind fields cannot be recovered due to the lack of vorticity information. To obtain a better understanding of the spatial variation of the MLT region wind fields, larger area observations (and hence higher meteor count rates) and measurements of the non-homogenous wind fields are needed. An extension of the classic monostatic meteor technique is required to satisfy these needs.

55 To resolve the limitations outlined above, the concept of multistatic meteor radar systems, such as MMARIA (multi-static and multi-frequency agile radar for investigations of the atmosphere) (Stober and Chau, 2015) and SIMO (single input multiple output) (Spargo et al., 2019), MIMO (multiple input multiple output radar) (Chau et al., 2019) have been designed and implemented (Stober et al., 2018). Multistatic systems can utilize the forward scatter of meteor trails, thus providing another perspective for observing the MLT. Multistatic meteor radar systems have many advantages over classic monostatic meteor 60 radars, such as obtaining higher-order wind fields information and covering wider observation areas. There have been some particularly innovative studies using multistatic meteor radar systems in recent years. For example, by combining MMARIA and the continuous wave multistatic radar technique (Vierinen et al., 2016), Stober and Chau et al. built a 5-station total 7-link multistatic radar network covering an approximately 600 km × 600 km region in Germany to retrieve an arbitrary non-

homogenous wind fields with a $30 \text{ km} \times 30 \text{ km}$ horizontal resolution (Stober et al., 2018). ~~Stober et al.~~ Chau et al. used two adjacent classic monostatic specular meteor radars in northern Norway to obtain horizontal divergence and vorticity (Chau et al., 2017). Other approaches, such as ~~the novel multistatic meteor radar data processing method coded continuous wave meteor radar~~ (Vierinen et al., 2019) and the compressed sense method in MIMO sparse signal recovery (Urco et al., 2019), are described in the references in these papers.

Analysing spatial resolution in ~~regions of interest~~ **interested areas** is a fundamental but difficult topic for meteor radar systems. Meteor radar systems transmit radio waves and then receive radio waves using a cluster of receiver antennas; commonly five antennas as in the Jones et al. configuration (Jones et al., 1998). By analysing the cross correlation of received signals, ~~we~~ **one** can determine the angle of arrivals (AoAs), ~~that is, which includes~~ the zenith angle and azimuth angle ~~denoted as~~ θ and ϕ respectively. By measuring the wave propagation time, **one** can obtain the range **information**. Most meteor radar systems rely on specular reflections from meteor trails. Thus, by combining the AoAs and the range information and then using geometric analysis, ~~we~~ **one** can determine the location of meteor trails. Accurately locating the meteor **trail specular point** (MTSP hereafter) is important since atmospheric parameter retrieval (such as the wind fields or the temperature) depends on the location information of meteor trails. The location accuracy, namely the spatial resolution, determines the reliability of the retrieved parameters. For multistatic meteor radar systems that can relax the assumption of a homogenous horizontal wind fields, the ~~resolution distribution~~ **location accuracy** becomes a more important issue because the horizontal spatial resolution affects the accuracy of the retrieved horizontal wind fields gradient.

There are some discussions about measuring errors of the meteor radar. There are For example, a number of studies have discussed AoAs measuring errors (Kang, 2008; Vaudrin et al., 2018; Younger and Reid, 2017). However, those ~~error analyses~~ discussions emphasize focus on the errors in receiver antennas and seldom discuss the influence of a multistatic configuration on the spatial resolutions. And those analyses consider the error propagation starting from the original signals received by the cluster of antennas. Therefore, the results of AoAs measuring errors become too intricate to utilize in further resolution analyses. Hocking developed a vertical resolution analysis method in a 2-dimensional baseline vertical section (Hocking, 2018), which simplifies the error propagation process in receiver antennas and put emphasis on how a bistatic meteor radar configuration would affect the vertical resolution in a vertical section. However, Hocking's method (HM hereafter) can barely show bistatic configurations' influence on spatial resolution distribution due to ignore the discussion of radial distance measuring error. Moreover, HM is only a demo about vertical resolution in a specific vertical section, not in real three-dimensional space. Hence, for practical purposes, the 3-dimensional spatial distribution of both horizontal resolution and vertical resolution should be considered.

Although multistatic meteor radar systems have developed well experimentally in recent years, the reliability of retrieved atmospheric parameters lacks discussion both for monostatic and multistatic meteor radar. A large part of the reason is that no other measurement technology can provide contrast data for meteor radars in MLT region. To better understand the reliability of the obtained atmospheric parameters, quantitative error analyses are necessary. On the one hand it proves that meteor radars are irreplaceable in MLT region as a measurement technology; on the other hand, to know the reliability of meteor radars

obtained atmospheric parameters and to get better understanding of the dynamic process in MLT region, some quantitative error analyses are necessary and helpful. In this paper, we analyse the multistatic meteor radar resolution distribution in a three-dimensional space for both vertical and horizontal resolution for the first time. And spatial resolution is a prerequisite for evaluating the reliability of retrieved atmospheric parameters, such as wind fields and temperature.

2 Analytical Method

2.1 brief introduction

The HM will be introduced ahead in short to help understand our method. In the HM, measuring errors that affect vertical resolution can be classified into two types (Hocking, 2018) : one is those that caused by the zenith angle measuring error $\delta\theta$ and another is those that caused by the pulse-length effect on vertical resolution. The receiver is reduced to a simple antenna pair that is collinear to the baseline (figure 1). HM only calculate vertical resolution in a two-dimensional vertical section which pass though the baseline. The receiver antenna pair is equivalent to one receiver arm in Jones configuration which is comprised of three collinear antennas and is usually in a 2λ \ 2.5λ configuration. The radio wave Phase difference of received radio wave between antenna pairs is denoted as $\Delta\Psi$. In meteor radar systems, there are is an acceptable phase difference measuring error (PDME hereafter) $\delta(\Delta\Psi)$. A higher value of $\delta(\Delta\Psi)$ means that more detected signals will be judged as a meteor event meanwhile more misidentifications and bigger errors as well. $\delta(\Delta\Psi)$ is usually set to approximately 30° (Hocking, 2018; Younger and Reid, 2017) in meteor radar systems. In the HM, the AoAs error the zenith angle measuring error $\delta\theta$ is due to $\delta(\Delta\Psi)$ and $\delta(\Delta\Psi)$ is a constant. Therefore, the error propagation in the receiver is very simple, and $\delta\theta$ is inversely proportional to the cosine of the zenith angle.

Now introduce our analytical method. Our method considers a multistatic system with multiple transmitters and one receiver in 3-dimensional space (figure 2). The receiving array receiver is in the Jones configuration, which can be “cross-shaped”, “T-shaped” or “L-shaped” in a plan view layout. The five receiver antennas are in the same horizontal plane and constitute two orthogonal antenna arms. To avoid a complex error propagation process in receiver and to place emphasis on multistatic configurations, the PDMEs in the two orthogonal antenna arms ($\delta(\Delta\Psi_1)$ and $\delta(\Delta\Psi_2)$) are constants. Therefore, the AoAs measuring errors (including zenith and azimuth angle measuring errors $\delta\theta$, $\delta\phi$ respectively) can be expressed as a simple function of zenith and azimuth angle. The radial distance is the distance between the MTSP and the receiver, which denoted as R_s . R_s can be determined by combining the AoAs, baseline length d_i , and the radio wave propagating path length R (Stober and Chau, 2015). See figure 4(a), if α , d_i and R are known, R_s will be calculated easily using Cosine Law as:

$$125 \quad R_s = \frac{R^2 - d_i^2}{2(R - d_i \cos\alpha)} \quad (1)$$

α is the angle between the baseline (i.e. axis- X_i) and the line from the receiver to the MTSP denoted as point A. The multistatic configuration will influence the accuracy of R_s (denoted as δR_s). This is because that α , d and R are determined by the multistatic configuration. We consider the error term δR_s in our method, which is ignored in the HM. δR_s is a function of the AoAs measuring errors ($\delta\theta$ and $\delta\phi$) and the radio wave propagation distance path length measuring error (denoted as δR). δR is caused by the measuring error of the wave propagation time δt , which is approximately $21\mu\text{s}$ (Kang, 2008). Thus, δR can be set as a constant and the default value in our program is $\delta R = c \delta t = 6.3\text{km}$. It is worth noting that the maximum unambiguous range for pulse meteor radars is determined by the pulse repetition frequency (PRF) (Hocking et al., 2001; Holdsworth et al., 2004). For multistatic meteor radars utilizing forward scatter, the maximum unambiguous range is c/PRF (where c is the speed of light). For the region area where R exceed the maximum unambiguous range, δR is set to positive infinity.

2.2 three kinds of coordinate systems and their transformations

To better depict the multistatic system configuration, we need to establish appropriate coordinate systems (figure 3). The spatial configuration of the receiver horizontal plane is determined by the local topography and the antenna configuration. We establish a left hand coordinate system XYZ to depict the receiver horizontal plane. XYZ is fixed on the receiver and thus will rotate with the 5 antenna horizontal plane. The coordinate origin of XYZ is on the receiver. Axis Z is collinear with the antenna boresight and perpendicular to the horizontal plane. Axis X and axis Y are in the horizontal plane and collinear with the arms of the two orthogonal antenna arrays. Therefore, the zenith angle and azimuth angle are conveniently represented in the XYZ coordinate system. For different transmitters T_t , the baseline direction and distance between T_t and the receiver are different. It is convenient to analyse the range information in the plane that goes through the baseline and meteor trail reflection points (figure 4). Thus, we establish a class of coordinate systems $X_t^t Y_t^t Z_t^t$ for each T_t . The coordinate origins of $X_t^t Y_t^t Z_t^t$ are all on the receiver. We stipulate that axis X_t^t points to transmitter i (T_i). Axis Y_t^t and axis Z_t^t need to satisfy the right hand corkscrew rule with axis X_t^t . Each transmitter, T_t , and the receiver constitute a radar link, which is referred to as L_t . We will deal with the range information for each L_t in $X_t^t Y_t^t Z_t^t$. Spatial resolution distributions for every L_t need to be compared in the same coordinate system, and this coordinate system needs to be convenient for retrieving wind fields. Therefore, we establish a local WNU (west north up) coordinate system $X_0^t Y_0^t Z_0^t$ on the receiver. The origin of $X_0^t Y_0^t Z_0^t$ is on the receiver with axis X pointing to the west, axis Y to the north, and axis Z pointing up. All spatial resolution distributions for each L_t will ultimately be converted to $X_0^t Y_0^t Z_0^t$.

To better depict the multistatic system configuration, three kinds of right-hand coordinate systems (figure 3) need to be established, which are $X_0 Y_0 Z_0$, $X_i Y_i Z_i$ and XYZ. $X_0 Y_0 Z_0$ is the ENU (east-north-up) coordinate system and axis- X_0 , Y_0 , Z_0 represent the east, north, up directions respectively. Another two coordinate systems are established to facilitate different error propagations. All types of errors need to be transformed to the ENU coordinate system $X_0 Y_0 Z_0$ in the end. Coordinate system XYZ is established to depict the spatial configuration of the receiver. XYZ is fixed on the receiver. See figure 3, the coordinate

origin of XYZ is on the receiver. Axis-Z is collinear with the antenna boresight and perpendicular to the receiver horizontal plane. Axis-X and axis-Y are collinear with the arms of the two orthogonal antenna arrays. AoAs will be represented in XYZ for convenience. See figure 4, it is convenient to analyse the range information in a plane that goes through the baseline and 160 MTSP. Thus, a coordinate system $X_iY_iZ_i$ is established for a transmitter T_i . The coordinate origins of $X_iY_iZ_i$ are all on the receiver. We stipulate that axis- X_i points to transmitter i (T_i). Each pair of T_i and the receiver R_X constitute a radar link, which is referred to as L_i . The range related information for each L_i will be calculated in $X_iY_iZ_i$. Different types of errors need to propagate to and be compared in $X_0Y_0Z_0$ which is convenient for retrieving wind fields.

165 We specify stipulate that clockwise rotation is satisfies the right-hand corkscrew rule. By rotating clockwise in order of $\psi_x^{x,i}$, $\psi_y^{y,i}$ and $\psi_z^{z,i}$ about axis-X, Y and Z, respectively, one can transform XYZ to $X_iY_iZ_i$. It is worth mentioning that $X_iY_iZ_i$ is non-unique because any rotation about axis- X_i can obtain another satisfactory $X_iY_iZ_i$. Hence, $\psi_x^{x,i}$ can be set to any values. Similarly, by rotating clockwise in order of $\psi_x^{i,0}$, $\psi_y^{i,0}$ and $\psi_z^{i,0}$ about axis-X, Y and Z, respectively, one can transform 170 $X_iY_iZ_i$ to $X_0Y_0Z_0$. To realize the coordinate transformation between those three coordinate systems, coordinate rotation matrix $A_R(\psi_x, \psi_y, \psi_z)$ is introduced. Using A_R , one can transform the coordinate point or vector presentation from one coordinate system to another. The details of the coordinate rotation matrix $A_R(\psi_x, \psi_y, \psi_z)$ can be seen in **Appendix (A.1)**.

2.3 two types of measuring errors

The analytical method of the spatial resolution of each radar link is the same. The difference between those radar links is 175 are only the value of the six coordinates rotation angle ($\psi_x^{x,i}$, $\psi_y^{y,i}$ and $\psi_z^{z,i}$; $\psi_x^{i,0}$, $\psi_y^{i,0}$ and $\psi_z^{i,0}$) and baseline distance d_i . In the following, we analyse the spatial resolution of one radar link, L_t as an example. The measurement errors, which affect the spatial resolution, cause a location bias in the specular reflection point. These errors The spatial resolution related measurement errors which will cause location errors of MTSP, can be classified into two types: E_1 is caused by measurement errors in the receiver, and E_2 is due to the pulse length. These two errors are mutually independent. Hence, the total error (E_{total}) in the form of the mean square error (MSE) can be expressed as:

$$180 \quad E_{total}^2 = E_1^2 + E_2^2 \quad (2)$$

E_1 is related to three indirect measuring errors. $\delta\theta$, $\delta\phi$ and δR_s , which They are zenith, azimuth and radial distance measuring errors, denoted as $\delta\theta$, $\delta\phi$ and δR_s respectively. In XYZ, E_1 can be decomposed into three orthogonal error vectors using $\delta\theta$, $\delta\phi$ and δR_s (figure 4(c)). Now we explain it in detail. $\delta\theta$ and $\delta\phi$ are the functions of PDMEs $\delta(\Delta\Psi_1)$ and $\delta(\Delta\Psi_2)$. $\Delta\Psi_1$ and $\Delta\Psi_2$ are theoretical phase difference of two orthogonal antenna arrays respectively. Those two 185 PDMEs $\delta(\Delta\Psi_1)$ and $\delta(\Delta\Psi_2)$ are treated as two independent measuring errors. PDMEs, i.e. $\delta(\Delta\Psi_1)$ and $\delta(\Delta\Psi_2)$, are caused by some practical factors, such as phase calibration mismatch and the fact that specular point is not actually a point but has a few Fresnel zones length. A meteor radar system calculates phase difference of different pair of antennas though cross-correlations and then fit them to get the most likely AoAs. Therefore, the system needs to set a tolerant value of $\delta(\Delta\Psi_1)$ and

$\delta(\Delta\Psi_2)$. Different meteor radar systems have different AoAs-fit algorithms and thus different AoAs measuring error distribution. To analyses the spatial resolution for a SIMO meteor radar system as common as possible and to avoid tedious error propagation in receiver, we start error propagation from $\delta(\Delta\Psi_1)$ and $\delta(\Delta\Psi_2)$ and set them as constant. AoAs measuring errors, i.e. $\delta\theta$ and $\delta\phi$ can be expressed as:

$$\delta\theta = \frac{\lambda}{2\pi D_1} \frac{\cos\phi}{\cos\theta} \delta(\Delta\Psi_1) + \frac{\lambda}{2\pi D_2} \frac{\sin\phi}{\cos\theta} \delta(\Delta\Psi_2) \quad (3)$$

$$\delta\phi = \frac{\lambda}{2\pi D_2} \frac{\cos\phi}{\sin\theta} \delta(\Delta\Psi_2) - \frac{\lambda}{2\pi D_1} \frac{\sin\phi}{\sin\theta} \delta(\Delta\Psi_1) \quad (4)$$

λ is wavelength used in the radar system the radio wave length. D_1 and D_2 are the length of the two orthogonal antenna arms. θ and ϕ are the zenith angle and the azimuth angle, respectively. The details can be seen in **Appendix (A.2)**. It is worth noting that $\delta\theta$ and $\delta\phi$ are not mutually independent. The Expectation value of their product is not identical to zero unless $\frac{E(\delta^2(\Delta\Psi_1))}{D_1^2}$ is equal to $\frac{E(\delta^2(\Delta\Psi_2))}{D_2^2}$.

The true error of δR_s can be expressed as a function of δR , $\delta\theta$ and $\delta\phi$ as:

$$\delta R_s = F(\delta R, \delta\theta, \delta\phi) = f_R(\theta, \phi)\delta R + f_\theta(\theta, \phi)\delta\theta + f_\phi(\theta, \phi)\delta\phi \quad (5)$$

$f_R(\theta, \phi)$, $f_\theta(\theta, \phi)$ and $f_\phi(\theta, \phi)$ are the weight functions of δR_s . δR is the wave propagating distance measuring error. The details about the weight function and deduction can be found in **Appendix (A.3)**. Obviously, δR_s is related to the geometry of the multistatic meteor radar system. Thus far, the true error vectors of See figure 4(c), E_1 can be decomposed into three orthogonal error vectors in coordinate XYZ, which are denoted as $\overrightarrow{\delta R_s}$, $\overrightarrow{R_s\delta\theta}$ and $\overrightarrow{R_s\sin\theta\delta\phi}$ (figure 4(e)). These three vectors can be expressed in XYZ as:

$$\overrightarrow{\delta R_s} = \delta R_s (\sin\theta\cos\phi, \sin\theta\sin\phi, \cos\theta)^T \quad (6)$$

$$\overrightarrow{R_s\delta\theta} = R_s \delta\theta (\cos\theta\cos\phi, \cos\theta\sin\phi, -\sin\theta)^T \quad (7)$$

$$\overrightarrow{R_s\sin\theta\delta\phi} = R_s \sin\theta \delta\phi (-\sin\phi, \cos\phi, 0)^T \quad (8)$$

E_2 is related to the geometry of the radio wave propagating path. A pulse transmitted by transmitter might be reflected anywhere within the a pulse length (figure 4(b)). Hence, there exists an unclear area, and we denote it as This causes a location error of MTSP, represented as an error vector \overrightarrow{DA} . where D is the median point of isosceles triangle ΔABC 's side BC. From the geometry relationship, the representation of the error vector \overrightarrow{DA} can be solved in $X_iY_iZ_i$ by using geometry relationship as:

$$\overrightarrow{DA} = \left(\frac{(2-a_1-a_2)x_i + d_i(a_2-1)}{2}, \frac{(2-a_1-a_2)y_i}{2}, \frac{(2-a_1-a_2)z_i}{2} \right)^T \quad (9)$$

215 S is half wave pulse length and $a_1 = \frac{R_s - S}{R_s}$. $a_2 = \frac{R_t - S}{R_t}$. d_t is the straight line distance between the receiver and T_t (baseline length). d_t is the baseline length. (x_i, y_i, z_i) is the coordinate value of a MTSP (i.e. point A in figure 4) in $X_i Y_i Z_i$. Details can be seen in **Appendix (A4)**

2.4 transform to ENU coordinate

Here, we introduced two types of errors in different coordinate systems, and we now need to transform them into local coordinates $X'_0 Y'_0 Z'_0$, which is convenient for analysing wind fields. The true error vectors $\overrightarrow{\delta R_t}$, $\overrightarrow{R_t \delta \theta}$ and $\overrightarrow{R_t \sin \theta \delta \phi}$ need two coordinate transformations, that is, from XYZ to $X'_t Y'_t Z'_t$ and then to $X'_0 Y'_0 Z'_0$. By deducing, the true error of E_t can be expressed as vector $(\delta_{(1)} X'_0, \delta_{(1)} Y'_0, \delta_{(1)} Z'_0)^T$ in $X'_0 Y'_0 Z'_0$

$$\begin{pmatrix} \delta_{(1)} X'_0 \\ \delta_{(1)} Y'_0 \\ \delta_{(1)} Z'_0 \end{pmatrix} = \begin{pmatrix} X'_0(\delta R_t) & X'_0(\delta \theta) & X'_0(\delta \phi) \\ Y'_0(\delta R_t) & Y'_0(\delta \theta) & Y'_0(\delta \phi) \\ Z'_0(\delta R_t) & Z'_0(\delta \theta) & Z'_0(\delta \phi) \end{pmatrix} \cdot \begin{pmatrix} f_R(0, \phi) & f_\theta(0, \phi) & f_\phi(0, \phi) \\ 0 & \frac{R_t}{\theta} & 0 \\ 0 & 0 & \frac{R_t \sin \theta}{\theta} \end{pmatrix} \cdot \begin{pmatrix} \delta R_t \\ \delta \theta \\ \delta \phi \end{pmatrix} \quad (10)$$

We denote the first term in the right formula as the error projection matrix, which transforms $\overrightarrow{\delta R_t}$, $\overrightarrow{R_t \delta \theta}$ and $\overrightarrow{R_t \sin \theta \delta \phi}$ in XYZ to axis X'_0 , Y'_0 and Z'_0 . The second matrix term is referred to as the error weight matrix, which can assemble $R_t \delta \theta$ and $\delta \phi$ to $\overrightarrow{\delta R_t}$, $\overrightarrow{R_t \delta \theta}$ and $\overrightarrow{R_t \sin \theta \delta \phi}$. The matrix details can be seen in **Appendix (A.5)**. However, $\delta \theta$ and $\delta \phi$ are not independent. To calculate the mean square error (MSE), we need to transform $\delta \theta$ and $\delta \phi$ into two independent errors: $\delta(\Delta \Psi_1)$ and $\delta(\Delta \Psi_2)$. Using eq. (3) and (4), we can transform vector $(\delta R_t, \delta \theta, \delta \phi)^T$ to three independent measuring errors δR , $\delta(\Delta \Psi_1)$ and $\delta(\Delta \Psi_2)$ as:

$$230 \quad \begin{pmatrix} \delta R \\ \delta \theta \\ \delta \phi \end{pmatrix} = \begin{pmatrix} 1 & 0 & 0 \\ -\frac{1}{2\pi} \cos \phi & \frac{1}{2\pi} \sin \phi & 0 \\ 0 & \frac{\cos \theta}{D_x} & \frac{\cos \theta}{D_x} \\ 0 & \frac{1}{2\pi} \sin \phi & \frac{1}{2\pi} \cos \phi \\ 0 & \frac{\sin \theta D_x}{D_x} & \frac{\sin \theta D_x}{D_x} \end{pmatrix} \begin{pmatrix} \delta R_t \\ \delta(\Delta \Psi_1) \\ \delta(\Delta \Psi_2) \end{pmatrix} \quad (11)$$

We denote the first term on the right as the base transformation matrix. We denote the dot product of the error projection matrix, error weight matrix and base transformation matrix as W_{EP} . We refer to W_{EP} as the error propagation matrix. W_{EP} is a 3×3 matrix, and we denote the element in it as W_{ij} . Then, we define $SW_{EP} = W_{ij}^2$. Thus, E_t in the form of MSE square can be expressed as vector $(\delta_{(1)}^2 X'_0, \delta_{(1)}^2 Y'_0, \delta_{(1)}^2 Z'_0)^T$ in $X'_0 Y'_0 Z'_0$

$$235 \quad \begin{pmatrix} \delta_{(1)}^2 X'_0 \\ \delta_{(1)}^2 Y'_0 \\ \delta_{(1)}^2 Z'_0 \end{pmatrix} = SW_{EP} \begin{pmatrix} \delta^2 R \\ \delta^2(\Delta \Psi_1) \\ \delta^2(\Delta \Psi_2) \end{pmatrix} \quad (12)$$

Here, two types of errors in different coordinate systems have been introduced. Now they need to be transformed to ENU coordinates $X_0Y_0Z_0$, which is convenient for comparing between different radar link and analysing wind fields. E_1 related error vectors, which are three orthogonal vectors $\overrightarrow{\delta R_s}$, $\overrightarrow{R_s\delta\theta}$ and $\overrightarrow{R_s\sin\theta\delta\phi}$ and represented in XYZ as eq.(6)-(8), need to be transformed from XYZ to $X_0Y_0Z_0$. To project $\overrightarrow{\delta R_s}$, $\overrightarrow{R_s\delta\theta}$ and $\overrightarrow{R_s\sin\theta\delta\phi}$ towards axis- X_0, Y_0, Z_0 respectively and reassemble them to form three new error vectors in axis- X_0, Y_0, Z_0 . Using coordinate rotation matrix $A_R^{(XYZ, X_0Y_0Z_0)} = A_R(\Psi_x^{i,0}, \Psi_y^{i,0}, \Psi_z^{i,0}) \cdot A_R(\Psi_x^{X,i}, \Psi_y^{Y,i}, \Psi_z^{Z,i})$ and eq.(6)-(8), the unit vectors of those three vectors can be represented in $X_0Y_0Z_0$ as:

$$\begin{pmatrix} X'_0(\delta R_s) & X'_0(\delta\theta) & X'_0(\delta\phi) \\ Y'_0(\delta R_s) & Y'_0(\delta\theta) & Y'_0(\delta\phi) \\ Z'_0(\delta R_s) & Z'_0(\delta\theta) & Z'_0(\delta\phi) \end{pmatrix} = A_R^{(XYZ, X_0Y_0Z_0)} \cdot \begin{pmatrix} \sin\theta\cos\phi & \cos\theta\cos\phi & -\sin\phi \\ \sin\theta\sin\phi & \cos\theta\sin\phi & \cos\phi \\ \cos\theta & -\sin\theta & 0 \end{pmatrix} \quad (10)$$

$(X'_0(\delta R_s), Y'_0(\delta R_s), Z'_0(\delta R_s))^T$, $(X'_0(\delta\theta), Y'_0(\delta\theta), Z'_0(\delta\theta))^T$, $(X'_0(\delta\phi), Y'_0(\delta\phi), Z'_0(\delta\phi))^T$ are unit vectors of $\overrightarrow{\delta R_s}$, $\overrightarrow{R_s\delta\theta}$ and $\overrightarrow{R_s\sin\theta\delta\phi}$ in $X_0Y_0Z_0$ respectively. We denote the 3×3 matrix in left side of the eq.(10) is denoted as P_{ij} for $i, j = 1, 2, 3$.

See eq.(6)-(8) and figure 4(c), the length of those three vectors, or error values in other words, are δR_s , $R_s\delta\theta$, $R_s\sin\theta\delta\phi$ as the function of δR , $\delta\theta$, $\delta\phi$. In order to reassemble them to new error vectors, transforming $\delta\theta$ and $\delta\phi$ into two independent errors $\delta(\Delta\Psi_1)$ and $\delta(\Delta\Psi_2)$ are needed because $\delta\theta$ and $\delta\phi$ are not independent. Using eq. (3) and (4), one can transform vector $(\delta R, \delta\theta, \delta\phi)^T$ to three independent measuring errors δR , $\delta(\Delta\Psi_1)$ and $\delta(\Delta\Psi_2)$. And thus $(\delta R_s, R_s\delta\theta, R_s\sin\theta\delta\phi)^T$ can be expressed as:

$$\begin{pmatrix} \delta R_s \\ R_s\delta\theta \\ R_s\sin\theta\delta\phi \end{pmatrix} = \begin{pmatrix} f_R(\theta, \phi) & f_\theta(\theta, \phi) & f_\phi(\theta, \phi) \\ 0 & R_s & 0 \\ 0 & 0 & R_s\sin\theta \end{pmatrix} \cdot \begin{pmatrix} 1 & 0 & 0 \\ 0 & \frac{\lambda}{2\pi} \frac{\cos\phi}{D_1} & \frac{\lambda}{2\pi} \frac{\sin\phi}{D_2} \\ 0 & -\frac{\lambda}{2\pi} \frac{\sin\phi}{D_1} & \frac{\lambda}{2\pi} \frac{\cos\phi}{D_2} \end{pmatrix} \cdot \begin{pmatrix} \delta R \\ \delta(\Delta\Psi_1) \\ \delta(\Delta\Psi_2) \end{pmatrix} \quad (11)$$

The product of the first and the second term in right side of eq.(11) is a 3×3 matrix, denoted as W_{ij} for $i, j = 1, 2, 3$. Seen eq.(11), three error values δR_s , $R_s\delta\theta$, $R_s\sin\theta\delta\phi$ are the linear combinations of three basis δR , $\delta(\Delta\Psi_1)$, $\delta(\Delta\Psi_2)$ with their corresponding linear coefficients W_{1j}, W_{2j}, W_{3j} . Those three error values can be projected toward new directions (i.e. axis- X_0, Y_0, Z_0) by using P_{ij} . It worth noting that in a new direction, a same basis's projected linear coefficients from different error values should be used to calculate their sum of squares (SS). And then the square root of SS will be used as a new linear coefficient for that basis in the new direction. For example, in X_0 directions, basis $\delta(\Delta\Psi_1)$'s projected linear coefficients are $X'_0(\delta R_s)W_{12}$, $X'_0(\delta\theta)W_{22}$, $X'_0(\delta\phi)W_{32}$ from $\overrightarrow{\delta R_s}$, $\overrightarrow{R_s\delta\theta}$ and $\overrightarrow{R_s\sin\theta\delta\phi}$ respectively. Therefore, the new linear coefficient for $\delta(\Delta\Psi_1)$ in X_0 direction is $W_{X'_0}^{\delta(\Delta\Psi_1)} = \pm\sqrt{(X'_0(\delta R_s)W_{12})^2 + (X'_0(\delta\theta)W_{22})^2 + (X'_0(\delta\phi)W_{32})^2}$. Similarly, one can get δR and $\delta(\Delta\Psi_2)$'s new linear coefficients in X'_0 , denoted as $W_{X'_0}^{\delta R}$ and $W_{X'_0}^{\delta(\Delta\Psi_2)}$. Thus true error values in X_0 direction

is $W_{X'_0}^{\delta R} \delta R + W_{X'_0}^{\delta(\Delta\Psi_1)} \delta(\Delta\Psi_1) + W_{X'_0}^{\delta(\Delta\Psi_2)} \delta(\Delta\Psi_2)$. Because $\delta R, \delta(\Delta\Psi_1), \delta(\Delta\Psi_2)$ are mutually independent, E_1 related mean square error (MSE) values in X_0 direction, denoted as $\delta_{(1)}X_0$, can be expressed as $\delta_{(1)}X_0 =$

265
$$\pm \sqrt{\left(W_{X'_0}^{\delta R} \delta R \right)^2 + \left(W_{X'_0}^{\delta(\Delta\Psi_1)} \delta(\Delta\Psi_1) \right)^2 + \left(W_{X'_0}^{\delta(\Delta\Psi_2)} \delta(\Delta\Psi_2) \right)^2}.$$

In short, E_1 related errors in ENU coordinate's three axis directions (denoted as $\delta_{(1)}X_0, \delta_{(1)}Y_0$ and $\delta_{(1)}Z_0$) can be expressed in the form of matrix as:

$$\begin{pmatrix} \delta_{(1)}^2 X_0 \\ \delta_{(1)}^2 Y_0 \\ \delta_{(1)}^2 Z_0 \end{pmatrix} = P_{ij}^2 \cdot W_{ij}^2 \cdot \begin{pmatrix} \delta^2 R \\ \delta^2(\Delta\Psi_1) \\ \delta^2(\Delta\Psi_2) \end{pmatrix} \quad (12)$$

270 E_2 related error vector \overrightarrow{DA} needs transformation from $X_iY_iZ_i$ to $X_0Y_0Z_0$. Therefore, E_2 related errors in ENU coordinate's three axis directions (denoted as $\delta_{(2)}X_0, \delta_{(2)}Y_0$ and $\delta_{(2)}Z_0$) can be expressed in the form of matrix as:

$$\begin{pmatrix} \delta_{(2)} X_0 \\ \delta_{(2)} Y_0 \\ \delta_{(2)} Z_0 \end{pmatrix} = \pm A_R(\Psi_x^{i,0}, \Psi_y^{i,0}, \Psi_z^{i,0}) \cdot \overrightarrow{DA} \quad (13)$$

E_1 and E_2 are mutually independent. By using eq.(1), the total MSE values in ENU coordinate's three axis directions (denoted as $\delta_{\text{total}}X_0, \delta_{\text{total}}Y_0$ and $\delta_{\text{total}}Z_0$) can be expressed in the form of matrix as:

$$\begin{pmatrix} \delta_{\text{total}}^2 X_0 \\ \delta_{\text{total}}^2 Y_0 \\ \delta_{\text{total}}^2 Z_0 \end{pmatrix} = \begin{pmatrix} \delta_{(1)}^2 X_0 \\ \delta_{(1)}^2 Y_0 \\ \delta_{(1)}^2 Z_0 \end{pmatrix} + \begin{pmatrix} \delta_{(2)}^2 X_0 \\ \delta_{(2)}^2 Y_0 \\ \delta_{(2)}^2 Z_0 \end{pmatrix} \quad (14)$$

275 In conclusion, for a radar link L_i and a MTSP represented as (x_0, y_0, z_0) in ENU coordinate system $X_0Y_0Z_0$, as figure 4(a) sketched, the location errors of this point in east, north and up directions ($\pm\delta_{\text{total}}X_0, \pm\delta_{\text{total}}Y_0$ and $\pm\delta_{\text{total}}Z_0$) can be calculated as follows: firstly, for a point (x_0, y_0, z_0) in $X'_0Y'_0Z'_0$, using A_R to transform it to $X_iY_iZ_i$ and denoted as (x_i, y_i, z_i) . Then in $X_iY_iZ_i$ calculate AoAs (θ and ϕ) and range information (R_s and R_i). Details of AoAs and range calculation can be seen in **Appendix (A.5)**. It's worth noting that AoAs are the angles relative to axis of XYZ. Secondly, in 280 XYZ using AoAs and eq.(3)-(8) to calculate E_1 's three orthogonal error vectors as figure 4(c) sketched; in $X_iY_iZ_i$ use range information and eq.(9) to calculate E_2 's error vector \overrightarrow{DA} as figure 4(b) sketched. Thirdly, project E_1 's three error vectors to $X_0Y_0Z_0$ by using eq.(10) and use eq.(11)-(12) to reassemble them to calculate E_1 related MSE values in direction of X_0, Y_0, Z_0 ; use eq.(13) to transform E_2 error vector from $X_iY_iZ_i$ to $X_0Y_0Z_0$. Finally, use eq. (14) to get the total location errors of a MTSP in (x_0, y_0, z_0) . Figure 5(a) describes the process above.

We wrote a program to study the method above. The program is written in python language and is presented in supplement. To calculate a special configuration of a multistatic radar system, we initially **need to** set six coordinate transformation angles ($\psi_x^{X,i}$, $\psi_y^{Y,i}$ and $\psi_z^{Z,i}$; $\psi_x^{i,0}$, $\psi_y^{i,0}$ and $\psi_z^{i,0}$) and baseline length (**straight line distance** \mathbf{d}_i) for each radar link L_i . For example, $\psi_x^{i,0} = \psi_y^{i,0} = 0$, $\psi_z^{i,0} = 30^\circ$ and $d_i = 250\text{km}$ means a transmitter T_i is 250km, 30° east by south of the receiver R_X ; 290 Further, $\psi_x^{X,i} = 5^\circ$, $\psi_y^{Y,i} = 0$, $\psi_z^{Z,i} = 0$ means one receiver arm (axis-Y) points to east by north 60° with 5° elevation. The interested detection area of multistatic meteor radar is usually from 70km to 110km in height and lager than $300\text{km} \times 300\text{km}$ in horizontal. In our program, this area needs to be divided into a spatial grid for sampling. The default value of the sampling grid length is 1km in height and 5km in meridian and zonal directions. After the settings mentioned above, the program will traverse those sampling grid nodes and calculate the location errors of each nodes as described in figure 5(a). Figure 5(b) 295 describe the parameter settings and traversal calculation process above. For a given setting of radar link L_i , the program will output the squared values of E_1 related, E_2 related and total MSE (E_{total}^2 : $\delta_{total}^2 X_0$, $\delta_{total}^2 Y_0$, $\delta_{total}^2 Z_0$; E_1^2 : $\delta_{(1)}^2 X_0$, $\delta_{(1)}^2 Y_0$, $\delta_{(1)}^2 Z_0$; E_2^2 : $\delta_{(2)}^2 X_0$, $\delta_{(2)}^2 Y_0$, $\delta_{(2)}^2 Z_0$). The location errors can be positive or negative and thus the spatial resolutions are twice the absolute value of location errors. For example, See figure 5(c), for a detected MTSP represented as (x_0, y_0, z_0) 300 in $X_0Y_0Z_0$, if $\delta_{total}^2 X_0$, $\delta_{total}^2 Y_0$, $\delta_{total}^2 Z_0$ equals 25, 16 and 9 km^2 respectively, it means that the actual position of MTSP could occur in an area which is ± 5 km, ± 4 km, ± 3 km around (x_0, y_0, z_0) with equally probability. The zonal, meridian and vertical resolution are 10 km, 8 km and 6 km respectively.

The HM analyses vertical resolution (corresponding to δZ_0 in our paper) only in a 2-dimensional vertical section (corresponding to the X_0Z_0 plane in our paper). To compare with Hocking's work, except $\psi_z^{i,0}$ set to be 180° , other five coordinate transformation angles are all set to zero with \mathbf{d} is equal to 300 km. The half wave pulse length S is set to 2 km and 305 $\delta(\Delta\Psi_1)$ to 35° . ~~Setting $\delta(\Delta\Psi_2)$ to zero and calculating in only the X_0Y_0 plane should have degraded our method into Hocking's 2-dimensional analysis method, but the settings above doesn't work~~ because Hocking's method ignores δR_s . In fact, Hocking's method considers only E_2 and $\overrightarrow{R_s\delta\theta}$ in the X_0Y_0 plane. Hence, we need to further set $f_R(\theta, \phi)$, $f_\theta(\theta, \phi)$ and $f_\phi(\theta, \phi)$ to be zero. Thus, our method totally degrades into Hocking's method. Hocking's results are shown in the 310 absolute value of vertical location error normalized relative to half wave pulse width, i.e. $|\delta Z_0|/S$. Hereafter, $|E|/S$ is referred to normalized spatial resolutions such as $\delta_{(1)} X_0$ and $\delta_{total} Y_0$, where E represent location errors in a direction. Thus, Spatial resolutions are $2S$ times normalized spatial resolutions. The normalized vertical resolution distributions are shown in figure 6(a). Our results are the same as those in Hocking's work (Hocking, 2018). The distribution of $\overrightarrow{R_s\delta\theta}$ related, E_2 related and total normalized vertical resolution **distributions** are shown in figure 6 from left to right, respectively. In most cases, E_2 is an order of magnitude smaller than $\overrightarrow{R_s\delta\theta}$. Only in the region directly above the receiver does E_2 have the same magnitude as 315 $\overrightarrow{R_s\delta\theta}$. In other words, only in the region directly above the receiver can E_2 influence the total resolution. E_2 is related to the

bistatic configuration, but $\overrightarrow{R_s \delta \theta}$ is not. Therefore, in the HM, the distribution of the total vertical resolution is changed slightly varying with \mathbf{d} . After adding the error term $\overrightarrow{\delta R_t}$, which is related to the bistatic configuration, the normalized total vertical spatial resolution distribution will change visibly varying with \mathbf{d} , as figure 7's first two rows show. The region between two black lines represents a trustworthy sampling volume for receiver because the elevation angle is beyond 30° with less influence of potential mutual antenna coupling or other obstacles in the surrounding. However, with the transmitter/receiver distance become longer, resolutions in this trustworthy sampling volume are not always acceptable. In figure 7's first row, the transmitter/receiver distance is 300 km and about half of the region between two black line have normalized vertical resolution values lager than 3 km. Because our analytical method can obtain spatial resolutions in 3-dimensional space, figure 7's third row show a perspective to the horizontal section in 90 km altitude for figure 7's second row.

To get an intuitionistic perspective to spatial resolution distribution in 3-dimensional space, figure 8 shows the normalized zonal, meridian and vertical spatial resolution distribution of a multistatic radar link whose transmitter/receiver is 180 km away and the transmitter is south by east 30° of the receiver. Classic monostatic meteor radar is a special case of a multistatic meteor radar system whose baseline length is zero. By setting the transmitter/receiver distance to be zero in our program, a monostatic meteor radar's spatial resolution can also be obtained. The spatial resolution distributions are highly symmetrical and correspond to the real characteristics of monostatic meteor radar (not shown in the text, can be seen in the supplement SF1). In the discussion above, the receiver and transmitter antennas are all coplanar. By setting $\psi_x^{X,i}$, $\psi_y^{Y,i}$ and $\psi_z^{Z,i}$ in our program, the non-coplanar receiver/transmitter-antennas situations can also be studied. Slightly tilting of the receiver horizontal plane (for example, set $\psi_x^{X,i} = \psi_y^{Y,i} = 5^\circ$) will cause horizontal spatial distributions to change (seen SF2 and SF3 in the supplement). In practical applications, like the Earth's curvature and local topography or receiver horizontal plane calibration error all will lead to the receiver horizontal plane tilting. Thus, this kind of slant tilting should also be taken into account for multistatic meteor radar systems. The details of parameter setting can be seen in the supplement.

As mentioned above, the AoAs errors analysis can be complex. Hence, We have greatly simplified the AoAs error propagation process in the receiver has been simplified to eq.(3)-(4) by using the constant PDMEs as the start of error propagation. This is for the sake of the adaptable of our method. Put emphasis on the multistatic configuration. If analysing AoAs errors starts from the original voltage signals, the error propagation process will change with a specific receiver interferometer configuration and a specific signal processing method. In practical situations for an unusual receiver antenna configuration or new original signal processing algorithm, we can establish an error propagation process based on the specific circumstances needs to be established. Substitute $\delta(\Delta\Psi_1)$ and $\delta(\Delta\Psi_2)$ into other mutually independent direct measuring errors in a practical situation, and then establishing a new AoAs error propagation to obtain $\delta\theta$ and $\delta\phi$. Or in other words, rewrite the second and third term in eq. (11) to the new established AoAs error propagation matrix and new mutually independent measuring errors respectively. Our analytical method can still work.

It worth noting that except the PDMEs as the start of the error propagation, all the analytical processes are built on the mathematic error propagations. PDMEs include the uncontrolled errors, such as the scattered wave from a few Fresnel zones

along meteor trails, phase calibration inaccuracy and noises. However, there are other error sources in practical situation. For 350 example, planes or lightning may make troubles for meteor radar's discrimination system. And interference of obstacles in surroundings will cause further measurement errors of AoAs. These issues are related to actual situations and beyond the scope of this text.

The trustworthy sampling volume is vital for a meteor radar system and it determines the detection area and which meteors could be used in wind retrievals. To avoid the influence of the mutual antenna coupling or the ground clutter, the elevation 355 angle of detection should beyond a threshold, for example 30° in general. The spatial resolution is another thing that affects the trustworthy sampling volume. See Figure 7 and SF4 in supplement, only the area of normalized vertical resolution values below 3 km are shown, which represents an acceptable sampling volume. With transmitter/receiver distance increasing, this sampling volume becomes smaller along with the vertical resolution in this volume reduced. This fact limits the transmitter/receiver distance for multistatic meteor radar. Measurement response is important for measuring meteor trails' 360 Doppler shift caused by the background wind. The measured Doppler shift is caused by the component of the wind fields in the Bragg Vector. The smaller the angle between Bragg vector and the wind fields is, the larger this Doppler shift is and meanwhile the higher SNR. The Bragg vector of the multistatic configuration is divergent from the receiver's line of sight. Monostatic meteor radars can only detect winds in radial direction, thus only the mean wind can be solved. By synthesizing 365 monostatic and multistatic the high order component of the wind fields can be solved. The bigger the angle between the Bragg vector and radial direction is, or more diversified Bragg vectors in other words, the more complete and accurate the wind fields will be observed. In short, the trustworthy sampling volume, measurement response and the angular diversity of the Bragg vector should both be taken into account in wind retrievals. The discussion of wind retrievals is beyond the scope of this text and will be in a future work.

370 4 Conclusion

In this study, we presented the preliminary results of our error analytic method. Our method can calculate the spatial resolution in the zonal, meridian and vertical direction for an arbitrary configuration in three-dimensional space. The true location of a detected MTSP can locate within the spatial resolution with equal probability. Higher values of spatial resolution mean that this region needs more meteor counts or averaging to obtain a reliable accuracy. Our method shows that the spatial 375 configuration of a multistatic system will greatly influence the spatial resolution distribution in ENU coordinates and thus will in turn influence the retrieval accuracy of atmospheric parameters such as wind fields. The multistatic meteor radar system's spatial resolution analysis is a key point in analysing the accuracy of retrieved wind and other parameters. The influence of spatial resolutions on wind retrieval will be discussed in the future work. Multistatic radar systems come in many types, and our work in this paper considers only single-input (single-antenna transmitter in each T_r) and multi-output (5-antenna 380 interferometric receiver) pulse radar systems. Although single-input multi-output (SIMO) pulse meteor radar is a classic meteor

radar system, other meteor radar systems, such as continuous wave radar systems and MISO (multiple-antenna transmitter and single-antenna receiver), show good experimental results and have some advantages over SIMO systems. Using different types of meteor radar systems to constitute the meteor radar network is the future trend and we will add the spatial resolution analyses of other system to the frame of our method in the future. We will validate and apply the error analyses of spatial resolution in 385 horizontal wind determination in a multistatic meteor radar system, which will be built soon in China.

Code availability. The program to calculate the 3D spatial resolution distributions are available in supplement.

Author contributions: W.Z, X.X, W.Y designed the study. W.Z deduced the formulas and wrote the program. W.Z wrote the 390 paper for the first version. X.X supervised the work and provided valuable comments. I.R revised the paper. All of the authors discussed the results and commented on the paper.

Competing interest. The authors declare no conflicts of interests

395 *Acknowledgements.* This work is supported by the B-type Strategic Priority Program of CAS Grant No. XDB41000000, the National Natural Science Foundation of China (41774158, 41974174, 41831071 and 41904135), the CNSA pre-research Project on Civil Aerospace Technologies No. D020105, the Fundamental Research Funds for the Central Universities, and the Open Research Project of Large Research Infrastructures of CAS “Study on the interaction between low/mid-latitude atmosphere and ionosphere based on the Chinese Meridian Project.” Thanks for Dr.Jia Mingjiao to provide advises and Zeng 400 jie to check equations in this manuscript.

Reference

Browning, K. A., and Wexler, R.: The Determination of Kinematic Properties of a Wind fields Using Doppler Radar, *Journal of Applied Meteorology*, 7, 105-113, 10.1175/1520-0450(1968)007<0105:Tdokpo>2.0.Co;2, 1968.

Ceplecha, Z., Borovička, J., Elford, W. G., ReVelle, D. O., Hawkes, R. L., Porubčan, V., and Šimek, M.: Meteor Phenomena and Bodies, *Space Science Reviews*, 84, 327-471, 10.1023/A:1005069928850, 1998.

405 Chau, J. L., Stober, G., Hall, C. M., Tsutsumi, M., Laskar, F. I., and Hoffmann, P.: Polar mesospheric horizontal divergence and relative vorticity measurements using multiple specular meteor radars, *Radio Science*, 52, 811-828, 10.1002/2016rs006225, 2017.

Chau, J. L., Urco, J. M., Vierinen, J. P., Volz, R. A., Clahsen, M., Pfeffer, N., and Trautner, J.: Novel specular meteor radar 410 systems using coherent MIMO techniques to study the mesosphere and lower thermosphere, *Atmos. Meas. Tech.*, 12, 2113-2127, 10.5194/amt-12-2113-2019, 2019.

Hocking, W. K., Fuller, B., and Vandepeer, B.: Real-time determination of meteor-related parameters utilizing modern digital technology, *Journal of Atmospheric and Solar-Terrestrial Physics*, 63, 155-169, 10.1016/s1364-6826(00)00138-3, 2001.

Hocking, W. K.: Spatial distribution of errors associated with multistatic meteor radar, *Earth, Planets and Space*, 70, 93, 10.1186/s40623-018-0860-2, 2018.

Holdsworth, D. A., Reid, I. M., and Cervera, M. A.: Buckland Park all-sky interferometric meteor radar, *Radio Science*, 39, 10.1029/2003rs003014, 2004.

Jacobi, C., Hoffmann, P., and Kürschner, D.: Trends in MLT region winds and planetary waves, Collm (52° N, 15° E), *Annales Geophysicae (ANGEOP)*, 2008.

Jia, M. J., Xue, X. H., Dou, X. K., Tang, Y. H., Yu, C., Wu, J. F., Xu, J. Y., Yang, G. T., Ning, B. Q., and Hoffmann, L.: A case study of A mesoscale gravity wave in the MLT region using simultaneous multi-instruments in Beijing, *Journal of Atmospheric and Solar-Terrestrial Physics*, 140, 1-9, 10.1016/j.jastp.2016.01.007, 2016.

Jones, J., Webster, A. R., and Hocking, W. K.: An improved interferometer design for use with meteor radars, *Radio Science*, 33, 55-65, 10.1029/97rs03050, 1998.

Kang, C.: Meteor radar signal processing and error analysis, 2008.

Philippe, W., and Corbin, H.: On the Analysis of Single-Doppler Radar Data, *Journal of Applied Meteorology - J APPL METEOROL*, 18, 532-542, 10.1175/1520-0450(1979)018<0532:OTAOSD>2.0.CO;2, 1979.

Reid, I. M.: SOME ASPECTS OF DOPPLER RADAR MEASUREMENTS OF THE MEAN AND FLUCTUATING COMPONENTS OF THE WIND-FIELD IN THE UPPER MIDDLE ATMOSPHERE, *Journal of Atmospheric and Terrestrial Physics*, 49, 467-484, 10.1016/0021-9169(87)90041-9, 1987.

Spargo, A. J., Reid, I. M., and MacKinnon, A. D.: Multistatic meteor radar observations of gravity-wave–tidal interaction over southern Australia, *Atmos. Meas. Tech.*, 12, 4791-4812, 10.5194/amt-12-4791-2019, 2019.

Stober, G., Sommer, S., Rapp, M., and Latteck, R.: Investigation of gravity waves using horizontally resolved radial velocity measurements, *Atmos. Meas. Tech.*, 6, 2893-2905, 10.5194/amt-6-2893-2013, 2013.

Stober, G., and Chau, J. L.: A multistatic and multifrequency novel approach for specular meteor radars to improve wind measurements in the MLT region, *Radio Science*, 50, 431-442, 10.1002/2014rs005591, 2015.

Stober, G., Chau, J. L., Vierinen, J., Jacobi, C., and Wilhelm, S.: Retrieving horizontally resolved wind fields using multistatic meteor radar observations, *Atmos. Meas. Tech.*, 11, 4891-4907, 10.5194/amt-11-4891-2018, 2018.

Urco, J. M., Chau, J. L., Weber, T., Vierinen, J. P., and Volz, R.: Sparse Signal Recovery in MIMO Specular Meteor Radars With Waveform Diversity, *Ieee Transactions on Geoscience and Remote Sensing*, 57, 10088-10098, 10.1109/tgrs.2019.2931375, 2019.

Vaudrin, C. V., Palo, S. E., and Chau, J. L.: Complex Plane Specular Meteor Radar Interferometry, *Radio Science*, 53, 112-128, 10.1002/2017rs006317, 2018.

Vierinen, J., Chau, J. L., Pfeffer, N., Clahsen, M., and Stober, G.: Coded continuous wave meteor radar, *Atmospheric Measurement Techniques*, 9, 829-839, 10.5194/amt-9-829-2016, 2016.

Vierinen, J., Chau, J. L., Charuvil, H., Urco, J. M., Clahsen, M., Avsarkisov, V., Marino, R., and Volz, R.: Observing Mesospheric Turbulence With Specular Meteor Radars: A Novel Method for Estimating Second-Order Statistics of Wind Velocity, *Earth and Space Science*, 6, 1171-1195, 10.1029/2019ea000570, 2019.

450 Xue, X. H., Dou, X. K., Lei, J., Chen, J. S., Ding, Z. H., Li, T., Gao, Q., Tang, W. W., Cheng, X. W., and Wei, K.: Lower thermospheric-enhanced sodium layers observed at low latitude and possible formation: Case studies, *Journal of Geophysical Research-Space Physics*, 118, 2409-2418, 10.1002/jgra.50200, 2013.

Yi, W., Xue, X. H., Reid, I. M., Younger, J. P., Chen, J. S., Chen, T. D., and Li, N.: Estimation of Mesospheric Densities at Low Latitudes Using the Kunming Meteor Radar Together With SABER Temperatures, *Journal of Geophysical Research-Space Physics*, 123, 3183-3195, 10.1002/2017ja025059, 2018.

455 Younger, J. P., and Reid, I. M.: Interferometer angle-of-arrival determination using precalculated phases, *Radio Science*, 52, 1058-1066, 10.1002/2017rs006284, 2017.

Appendix

A.1 Coordinates rotation matrix

460 For a right-handed rectangular coordinate system XYZ , we rotate clockwise Ψ_x about axis-x to obtain a new coordinate Z' . We specify that clockwise rotation [satisfies](#) in the right-hand screw rule. A vector in XYZ , denoted as $(x, y, z)^T$, is represented as $(x', y', z')^T$ in [the new coordinate](#)- Z' . The relationship between $(x, y, z)^T$ and $(x', y', z')^T$ is:

$$\begin{pmatrix} x' \\ y' \\ z' \end{pmatrix} = A_x(\psi_x) \begin{pmatrix} x \\ y \\ z \end{pmatrix} = \begin{pmatrix} 1 & 0 & 0 \\ 0 & \cos\psi_x & \sin\psi_x \\ 0 & -\sin\psi_x & \cos\psi_x \end{pmatrix} \begin{pmatrix} x \\ y \\ z \end{pmatrix} \quad (\text{A1.1})$$

Similarly, we rotate clockwise Ψ_y about axis-y to obtain a new coordinate. The presentation for a vector in new coordinates 465 and original can be linked by a matrix, $A_y(\psi_y)$:

$$A_y(\psi_y) = \begin{pmatrix} \cos\psi_y & 0 & -\sin\psi_y \\ 0 & 1 & 0 \\ \sin\psi_y & 0 & \cos\psi_y \end{pmatrix} \quad (\text{A1.2})$$

we rotate clockwise Ψ_z about axis-z to obtain a new coordinate. The presentation for a vector in new coordinates and original can be linked by a matrix, $A_z(\psi_z)$:

$$A_z(\psi_z) = \begin{pmatrix} \cos\psi_z & \sin\psi_z & 0 \\ -\sin\psi_z & \cos\psi_z & 0 \\ 0 & 0 & 1 \end{pmatrix} \quad (\text{A1.3})$$

470 For any two coordinate systems XYZ and $X'Y'Z'$ with co-origin, one can always rotate clockwise Ψ_x , Ψ_y and Ψ_z in order of axis-X, Y, Z respectively, transforming XYZ to $X'Y'Z'$ (figure A.1). The presentation for a vector in $X'Y'Z'$ and XYZ can be linked by a matrix, $A_R(\psi_x, \psi_y, \psi_z)$:

$$A_R(\psi_x, \psi_y, \psi_z) = A_z(\psi_z)A_y(\psi_y)A_x(\psi_x) = \begin{pmatrix} \cos\psi_y\cos\psi_z & \sin\psi_x\sin\psi_y\cos\psi_z + \cos\psi_x\sin\psi_z & -\cos\psi_x\sin\psi_y\cos\psi_z + \sin\psi_x\sin\psi_z \\ -\cos\psi_y\sin\psi_z & -\sin\psi_x\sin\psi_y\sin\psi_z + \cos\psi_x\cos\psi_z & \cos\psi_x\sin\psi_y\sin\psi_z + \sin\psi_x\cos\psi_z \\ \sin\psi_y & -\sin\psi_x\cos\psi_y & \cos\psi_x\cos\psi_y \end{pmatrix} \quad (\text{A1.4})$$

475 We call $A_R(\psi_x, \psi_y, \psi_z)$ as the coordinates rotation matrix.

A.2 AoAs measuring errors

In coordinate XYZ , AoAs includes zenith angle θ and azimuth angle ϕ . The AoAs is determined by two phase difference $\Delta\Psi_1$ and $\Delta\Psi_2$. Taking one antenna array as an example and Assuming In the plane wave approximation, the radio wave is at angle γ_1 and γ_2 with an antenna array (figure A.2). There is a phase difference $\Delta\Psi_1$ and $\Delta\Psi_2$ between two antennas (figure 480 1). See figure 1, $\Delta\Psi_1$ and $\Delta\Psi_2$ can be expressed as:

$$\Delta\Psi_1 = \frac{2\pi D_1 \cos\gamma_1}{\lambda} \quad (\text{A2.1})$$

$$\Delta\Psi_2 = \frac{2\pi D_2 \cos\gamma_2}{\lambda} \quad (\text{A2.2})$$

Using γ_1 , γ_2 the AoAs can be expressed as:

$$\cos^2\gamma_1 + \cos^2\gamma_2 + \cos^2\theta = 1 \quad (\text{A2.3})$$

$$485 \quad \tan\phi = \frac{\cos\gamma_2}{\cos\gamma_1} \quad (\text{A2.4})$$

Or in another kind of expression:

$$\cos\gamma_1 = \sin\theta\cos\phi \quad (\text{A2.5})$$

$$\cos\gamma_2 = \sin\theta\sin\phi \quad (\text{A2.6})$$

substitute $\cos\gamma_1$ and $\cos\gamma_2$ in (A2.3) and (A2.4) by using (A2.1) and (A2.2):

$$490 \quad \cos^2\theta = 1 - \left(\frac{\lambda}{2\pi}\right)^2 \left(\frac{\Delta^2\Psi_1}{D_1^2} + \frac{\Delta^2\Psi_2}{D_2^2}\right) \quad (\text{A2.7})$$

$$\ln(\tan\phi) = \ln(D_1\Delta\Psi_2) - \ln(D_2\Delta\Psi_1) \quad (\text{A2.8})$$

(A2.7) and (A2.8) are the equations that link the phase difference with the AoAs and For (A2.7) and (A2.8), Using Taylor expanding θ and ϕ , $\Delta\Psi_1$ and $\Delta\Psi_2$ to first order:

$$2\cos\theta\sin\theta\delta\theta = \left(\frac{\lambda}{2\pi}\right)^2 \left[\frac{2\Delta\Psi_1\delta(\Delta\Psi_1)}{D_1^2} + \frac{2\Delta\Psi_2\delta(\Delta\Psi_2)}{D_2^2} \right] \quad (\text{A2.9})$$

$$495 \quad \delta\phi = \frac{\sin\phi\cos\phi}{\Delta\Psi_2}\delta(\Delta\Psi_2) - \frac{\sin\phi\cos\phi}{\Delta\Psi_1}\delta(\Delta\Psi_1) \quad (\text{A2.10})$$

For (A2.9) and (A2.10), substitute $\Delta\Psi_1$ and $\Delta\Psi_2$ using (A2.1), (A2.2) and (A2.5), (A2.6) to the functions of θ , ϕ . we get eq. (3) and eq. (4). Now, eq. (3) and eq. (4) have been proven. If the zenith angle $\theta = 0^\circ$, we stipulate that $\frac{\cos\phi}{\sin\theta}$ and $\frac{\sin\phi}{\sin\theta}$ are 1.

A.3 Radial distance measuring error

Expand R_s , R and $\cos\alpha$ in eq.(1) to first order, δR_s can be expressed as a function of δR and $\delta(\cos\alpha)$:

$$500 \quad \delta R_s = \frac{R^2 - 2Rd\cos\alpha + d^2}{2(R-d\cos\alpha)^2} \delta R + \frac{d(R^2 - d^2)}{2(R-d\cos\alpha)^2} \delta(\cos\alpha) \quad (\text{A3.1})$$

α is the angle between R_s and axis- X_i . We denote the zenith and azimuth angles in coordinate- $X_iY_iZ_i$ as θ' and ϕ' , respectively. And the relationship between α and θ' , ϕ' is

$$\cos\alpha = \sin\theta'\cos\phi' \quad (\text{A3.2})$$

Using coordinates rotation matrix $A_R(\psi_x^{X,i}, \psi_y^{Y,i}, \psi_z^{Z,i})$, $\sin\theta'\cos\phi'$ can be expressed as the function of AoAs:

$$505 \quad \sin\theta'\cos\phi' = A_{11}\sin\theta\cos\phi + A_{12}\sin\theta\sin\phi + A_{13}\cos\theta \quad (\text{A3.3})$$

A_{ij} are represent the elements in matrix $A_R(\psi_x^{X,i}, \psi_y^{Y,i}, \psi_z^{Z,i})$ for $i, j = 1, 2, 3$.

Using (A3.2) and (A3.3), $\delta(\cos\alpha)$ can be expressed as a function of $\delta\theta$ and $\delta\phi$ as:

$$\delta(\cos\alpha) = (A_{11}\cos\theta\cos\phi + A_{12}\cos\theta\sin\phi - A_{13}\sin\theta)\delta\theta + (-A_{11}\sin\theta\sin\phi + A_{12}\sin\theta\cos\phi)\delta\phi \quad (\text{A3.4})$$

Finally, δR_s can be expressed as the function of $\delta R, \delta\theta, \delta\phi$ as:

$$510 \quad \delta R_s = F(\delta R, \delta\theta, \delta\phi) = f_R(\theta, \phi)\delta R + f_\theta(\theta, \phi)\delta\theta + f_\phi(\theta, \phi)\delta\phi \quad (\text{A3.5})$$

For:

$$f_R(\theta, \phi) = \frac{d^2 + R^2 - 2Rd(A_{11}\sin\theta\cos\phi + A_{12}\sin\theta\sin\phi + A_{13}\cos\theta)}{2[R - d(A_{11}\sin\theta\cos\phi + A_{12}\sin\theta\sin\phi + A_{13}\cos\theta)]^2} \quad (\text{A3.6})$$

$$f_\theta(\theta, \phi) = \frac{d(R^2 - d^2)(A_{11}\cos\theta\cos\phi + A_{12}\cos\theta\sin\phi - A_{13}\sin\theta)}{2[R - d(A_{11}\sin\theta\cos\phi + A_{12}\sin\theta\sin\phi + A_{13}\cos\theta)]^2} \quad (\text{A3.7})$$

$$f_\phi(\theta, \phi) = \frac{d(R^2 - d^2)(-A_{11}\sin\theta\sin\phi + A_{12}\sin\theta\cos\phi)}{2[R - d(A_{11}\sin\theta\cos\phi + A_{12}\sin\theta\sin\phi + A_{13}\cos\theta)]^2} \quad (\text{A3.8})$$

515 **A.4 True error of E_2**

See figure 4 (b), the total length of side AC and side AB represents the pulse width. Side AC equals side CB and they both equal to half of the pulse width denoted as S . In $X_iY_iZ_i$, the presentation of point A is (x_i, y_i, z_i) , the receiver is $(0,0,0)$ and T_i is $(d,0,0)$. The distance between T_i and A is $R_i = R - R_s$. We denote that the presentation of point B and C in $X_iY_iZ_i$ is (x_B, y_B, z_B) and (x_C, y_C, z_C) , respectively. We use vector collinear to establish equations for B and C. Therefore, one can 520 obtain the coordinates of point B and C by the following equations:

$$(x_B, y_B, z_B)^T = \frac{R_s - S}{R_s} (x_i, y_i, z_i)^T \quad (A4.1)$$

$$(x_C - d, y_C, z_C)^T = \frac{R_i - S}{R_i} (x_i - d, y_i, z_i)^T \quad (A4.2)$$

For isosceles triangle ABC, the perpendicular line AD intersects side CB in middle point D. Then, we obtain the coordinate value of D in $X_iY_iZ_i$ as:

$$525 \quad (x_D, y_D, z_D) = \frac{1}{2}(x_B + x_C, y_B + y_C, z_B + z_C) = \frac{1}{2}((a_1 + a_2)x_i - a_2d + d, (a_1 + a_2)y_i, (a_1 + a_2)z_i) \quad (A4.3)$$

We denote $a_1 = \frac{R_s - S}{R_s}$, $a_2 = \frac{R_i - S}{R_i}$. Finally, one can obtain the error vector of E_2 as vector \overrightarrow{DA} in $X_iY_iZ_i$:

$$\overrightarrow{DA} = \left(\frac{(2-a_1-a_2)x_i + d(a_2-1)}{2}, \frac{2-a_1-a_2}{2}y_i, \frac{2-a_1-a_2}{2}z_i \right)^T \quad (A4.4)$$

A.5 calculate AoAs and range information in $X_iY_iZ_i$

530 For a space point (x_i, y_i, z_i) in $X_iY_iZ_i$ which represent a MTSP, R_s can be solved easily as:

$$\overrightarrow{R_s} = (x_i, y_i, z_i)$$

$$R_s = \sqrt{x_i^2 + y_i^2 + z_i^2} \quad (A6.1)$$

The distance between transmitter T_i and receiver R_X is d_i as sketched in figure 4(a). Thus, coordinate value of T_i in $X_iY_iZ_i$ is $(d_i, 0, 0)$ and R_i can be solved as:

$$535 \quad R_i = \sqrt{(x_i - d_i)^2 + y_i^2 + z_i^2} \quad (A6.2)$$

Before we calculate AoAs in $X_iY_iZ_i$, the representation of unit vectors of axis-X, Y, Z in $X_iY_iZ_i$ need to know. In XYZ those unit vectors are easily represented as $(1,0,0)^T$, $(0,1,0)^T$, $(0,0,1)^T$. Though coordinates rotation matrix $A_R(\psi_x^{X,i}, \psi_y^{Y,i}, \psi_z^{Z,i})$, one can get those unit vector's representation in $X_iY_iZ_i$ as:

$$\overrightarrow{n_x} = (A_{11}, A_{21}, A_{31})^T$$

540 $\vec{n}_y = (A_{12}, A_{22}, A_{32})^T$

$\vec{n}_z = (A_{13}, A_{23}, A_{33})^T$ (A6.3)

For \vec{n}_x , \vec{n}_y and \vec{n}_z are unit vectors of Axis-X, Y, Z respectively. And A_{ij} are the elements in 3×3 matrix $A_R(\psi_x^{X,i}, \psi_y^{Y,i}, \psi_z^{Z,i})$ for $i, j = 1, 2, 3$. Now AoAs can get as:

$$\cos \theta = \frac{\vec{R}_s}{R_s} \cdot \vec{n}_z \quad (\text{A6.4})$$

545 $\sin \theta = \sqrt{1 - \cos^2 \theta}$

(A6.5)

$$\cos \phi = \frac{\vec{R}_s}{R_s} \cdot \frac{\vec{n}_x}{\sin \theta}$$

(A6.6)

$$\sin \phi = \frac{\vec{R}_s}{R_s} \cdot \frac{\vec{n}_y}{\sin \theta} \quad (\text{A6.7})$$

550 For $0^\circ < \theta < 180^\circ$ and $0^\circ \leq \phi < 360^\circ$. When $\theta = 0^\circ$, we handle it as same as in **Appendix (A.2)**.

555

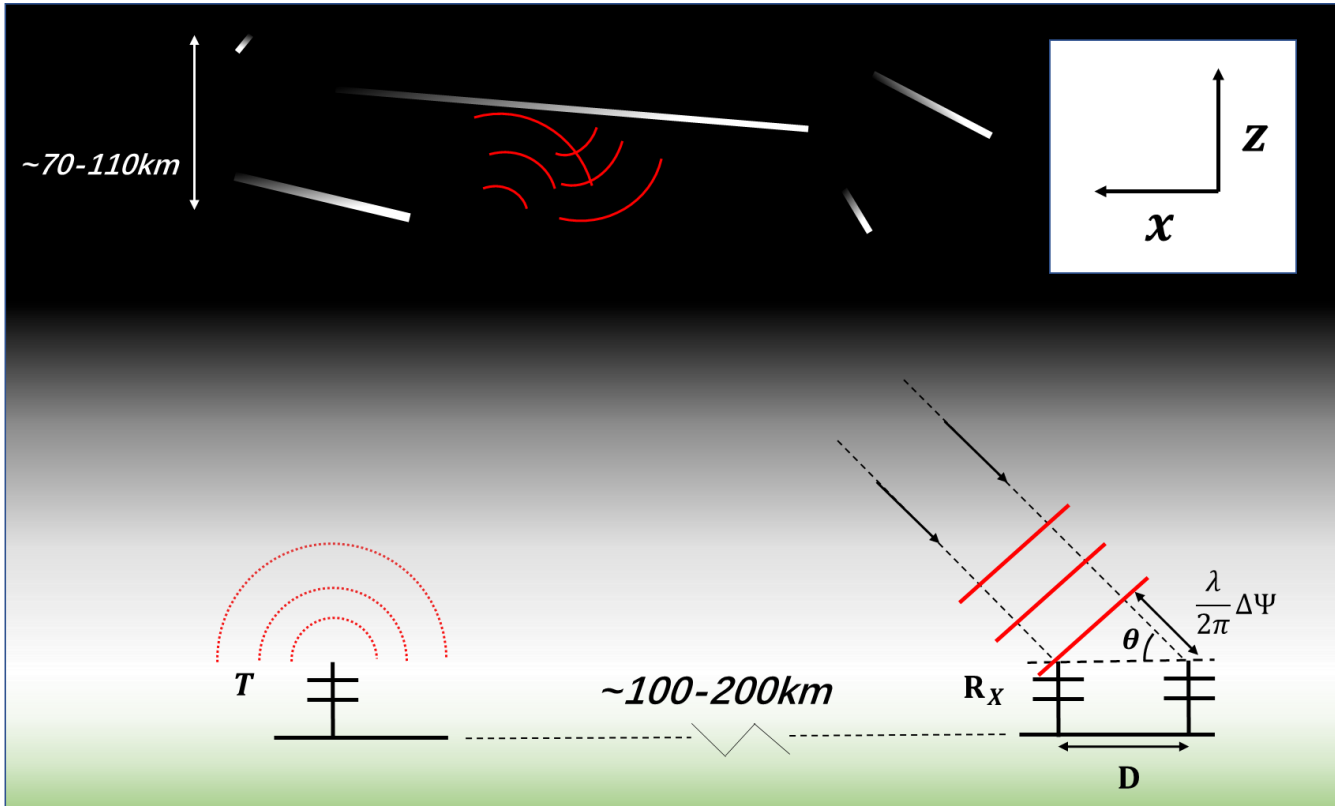


Figure 1: Schematic diagram of a simplified bistatic configuration used in Hocking's vertical resolution analysis(Hocking, 2018). The two receiver antennas and a transmitter antenna are collinear. The analysis is in a 2-dimensional vertical section through the baseline. The radio wave is scattered by a few Fresnel zones of several kilometres long around specular point in meteor trail and received by receiver antennas. The cross-correlation analysis between receiver antennas can solve the AoAs. The fact that the radio wave bounced back from a few Fennel zones will cause the measured phase difference between the receiver antenna pair deviating from the ideal phase difference. The ideal phase difference will solve an AoAs pointing to MTSP. This deviation from the ideal phase difference is one of the error sources of PDME.

560

565

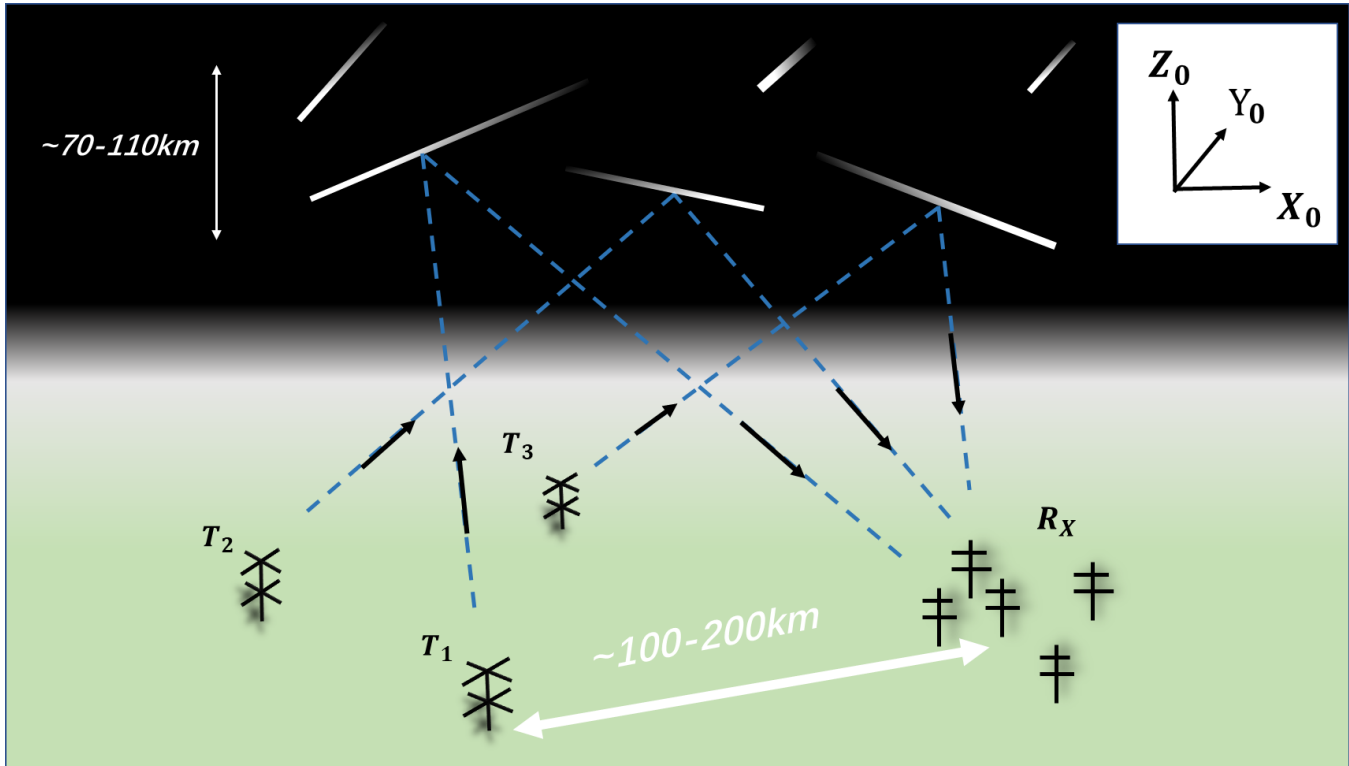


Figure 2: Schematic diagram of a multistatic meteor radar system using SIMO (single-input and multi-output). There are three transmitters (T_1 , T_2 and T_3) and one receiver (R_X) in the picture. The transmitter/receiver distance is usually approximately 100-200 km. X_0 , Y_0 , Z_0 represents the east, north and up directions of the receiver. Over 90% of the received energy comes from about one kilometre around specular point of the meteor trail, which is slightly less than the length of the central Fresnel zone (Ceplecha et al., 1998).

575

580

585

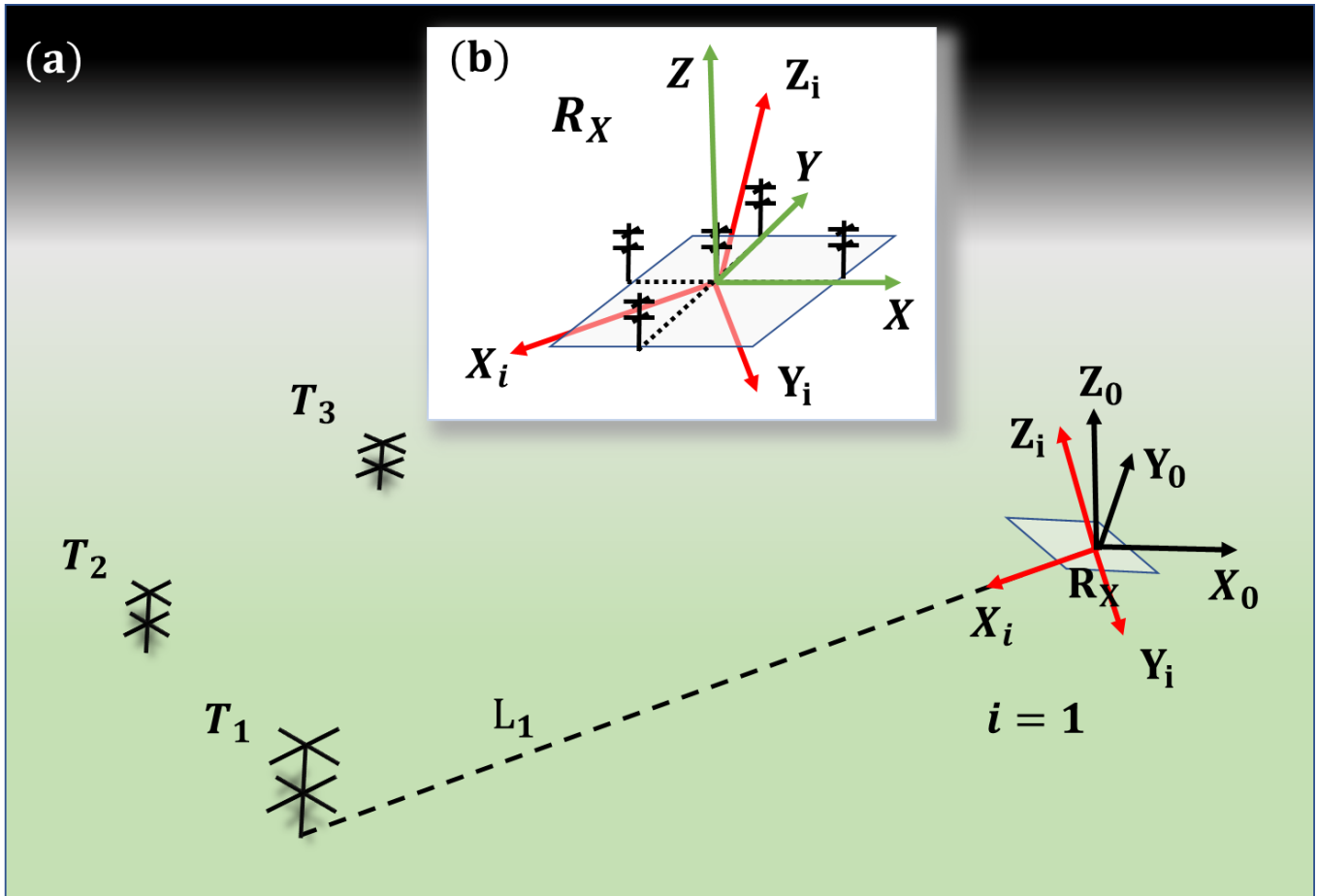


Figure 3: (a) Schematic diagram of the three introduced coordinate systems. $X_i Y_i Z_i$ are a class of coordinate systems whose axis- X_i point to transmitter i . And in this picture, i are 1,2,3. $X_0 Y_0 Z_0$ is the ENU coordinate system and all errors will be compared in this coordinate. (b) Magnified plot of the receiver. XYZ is fixed on the receiver horizontal plane. Axis-X and Y are collinear to two antenna arrays.

595

600

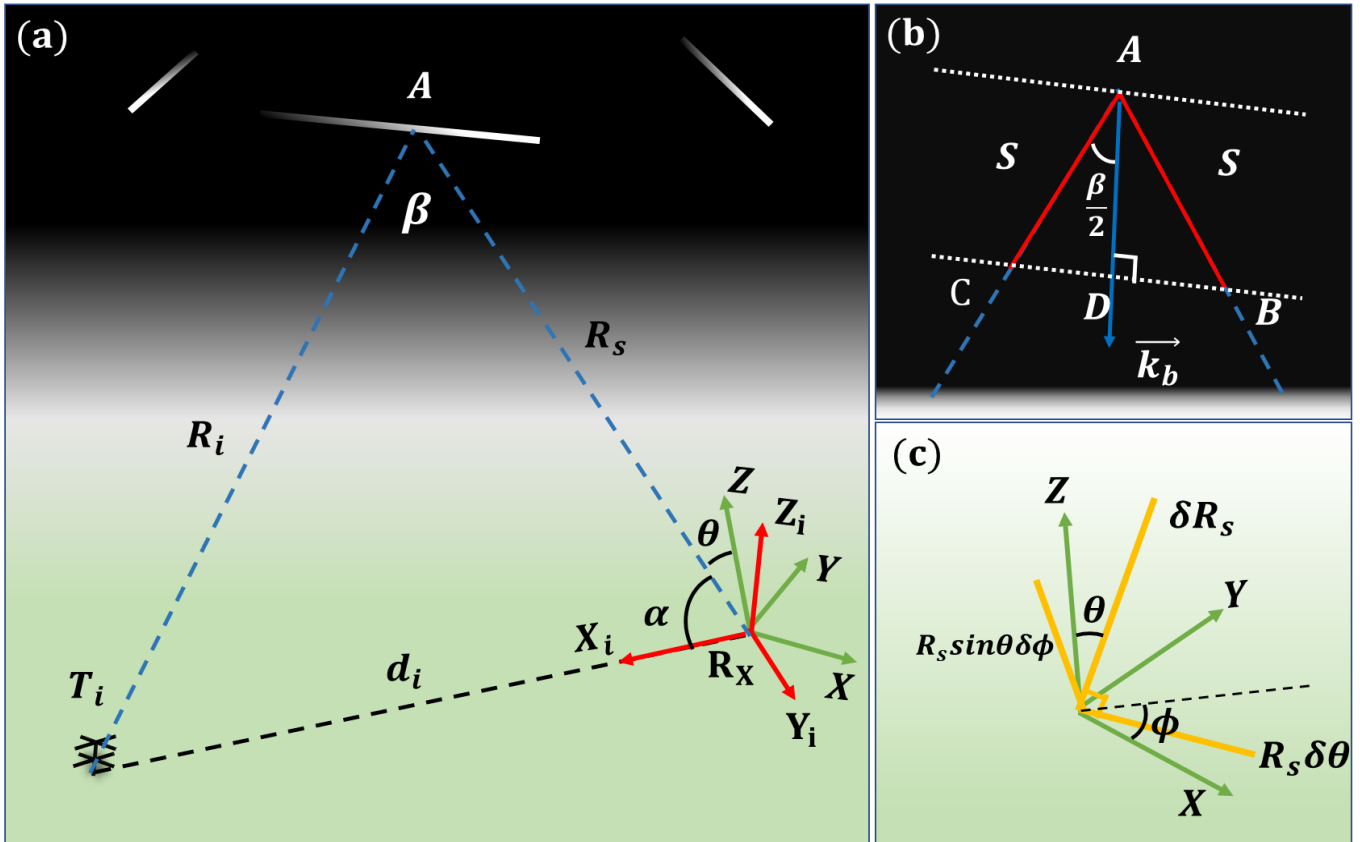
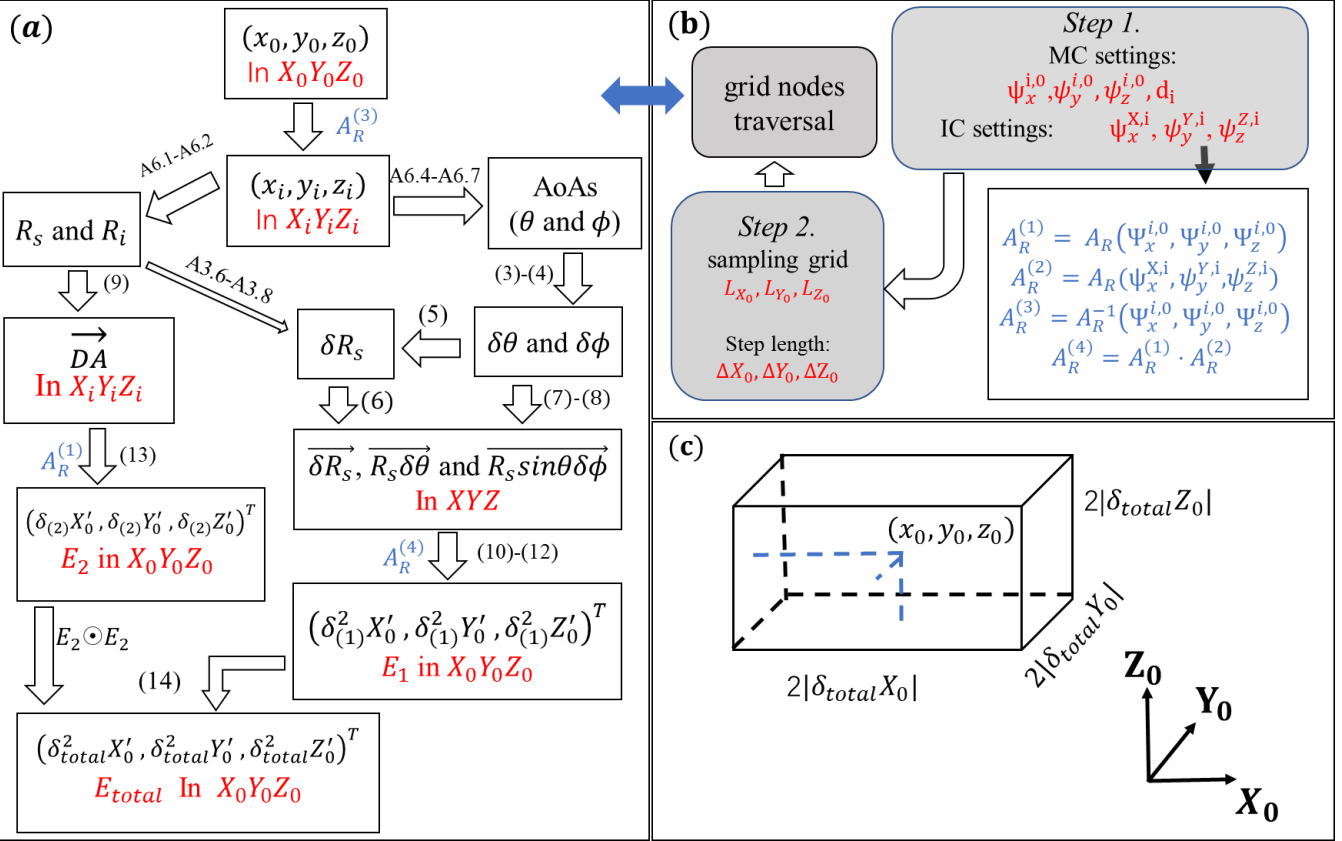


Figure 4: (a) Schematic diagram of a forward scatter geometry for the radar link between T_i and R_X . Point-A is the MTSP. (b) Magnified plot of specular point A. The red line represents a radio wave pulse, and S is the half wave pulse length. \vec{k}_b is the Bragg vector which halves forward scatter angle β . (c) Schematic diagram of E_1 in XYZ , which can be decomposed into three orthogonal vectors.

610

615



625

Figure 5: (a) the flow chart of the location error calculation process for a point in $X_0Y_0Z_0$. The marks beside arrows represent the corresponding equations (black) or coordinate rotation matrix (blue) in the paper. “ \odot ” is the Hadamard product. Thus $E_2 \odot E_2$ will get $(\delta_{(2)}^2 X_0, \delta_{(2)}^2 Y_0, \delta_{(2)}^2 Z_0)^T$. (b) the flow chart of the program to calculate the location errors distributions for a radar link L_i . This process includes parameters settings for a radar link, generating sampling grid nodes and traversing all the nodes. For each node, the program uses the calculation method described in (a). MC: multistatic configuration, IC: interferometer (receiver antennas) configuration. (c) Schematic diagram of relationship between the spatial resolution and the total location errors of the MTSP. For a detected point in space, the MSE of MTSP’s location errors is $\pm|\delta_{total}X_0|$, $\pm|\delta_{total}Y_0|$, $\pm|\delta_{total}Z_0|$ in zonal, meridian and vertical respectively. This means that the actual specular point might occur in a region which form a $2|\delta_{total}X_0| \times 2|\delta_{total}Y_0| \times 2|\delta_{total}Z_0|$ cube and the detected point is on the central of this cube.

630

635

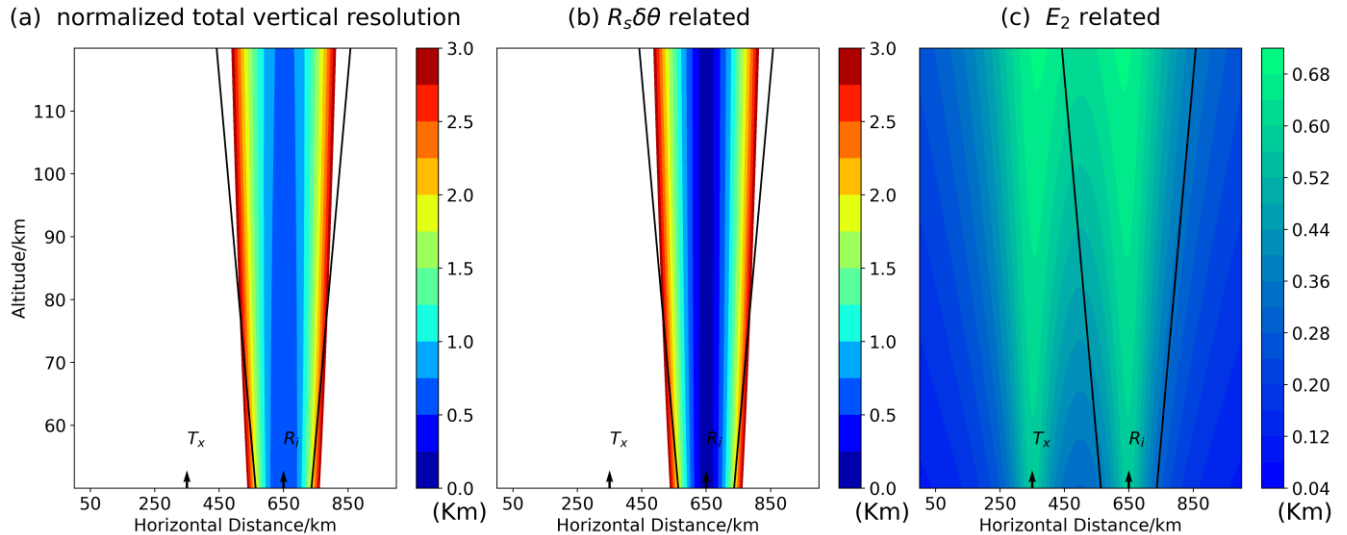


Figure 6: the normalized vertical resolution distribution in a vertical section from 50 km to 60 km height when ignore the error term “ δR_s ”. (a), (b), (c) are total, $R_s\delta\theta$ related and E_2 related normalized resolution distribution respectively. The results is the same as Hocking’s work (Hocking, 2018). Two black arrows represent the positions right above transmitter and receiver and transmitter/receiver are 300 km away. The region between two black oblique lines is the trustworthy sampling volume for the receiver because the elevation angle is beyond 30° with little influence of from potential mutual antenna coupling or other obstacles in the surrounding. Except the region in large elevation angle (i.e. 90°), E_2 related resolution values are much lower than $R_s\delta\theta$ related. $R_s\delta\theta$ related resolution distribution is only depend on the receiver. Thus, the total vertical resolution distribution is nearly unchanged with transmitter/receiver distance varying. The normalized resolution values exceed 3 km which correspond 12 km vertical resolution aren’t shown.

640

645

650

655

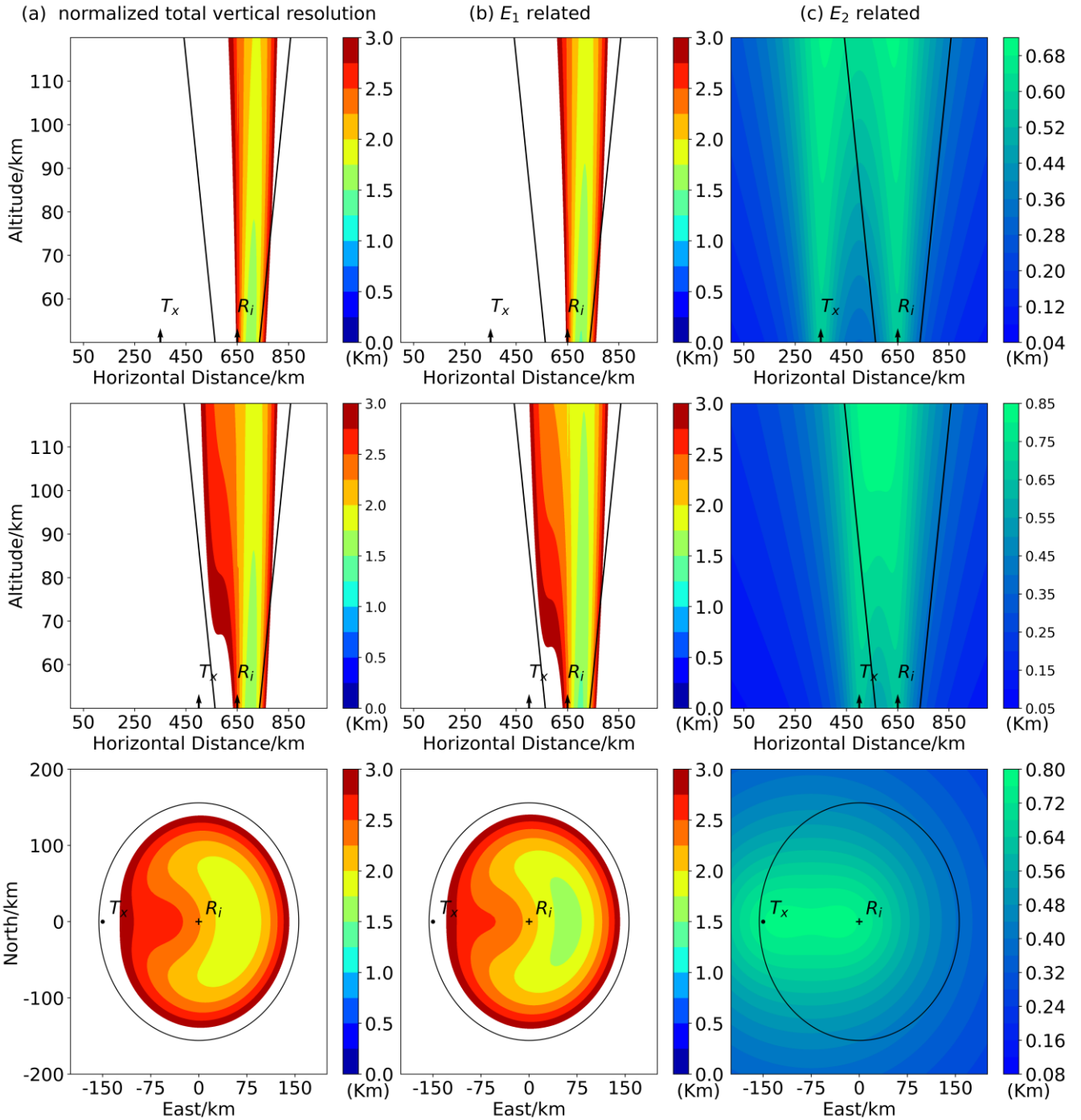
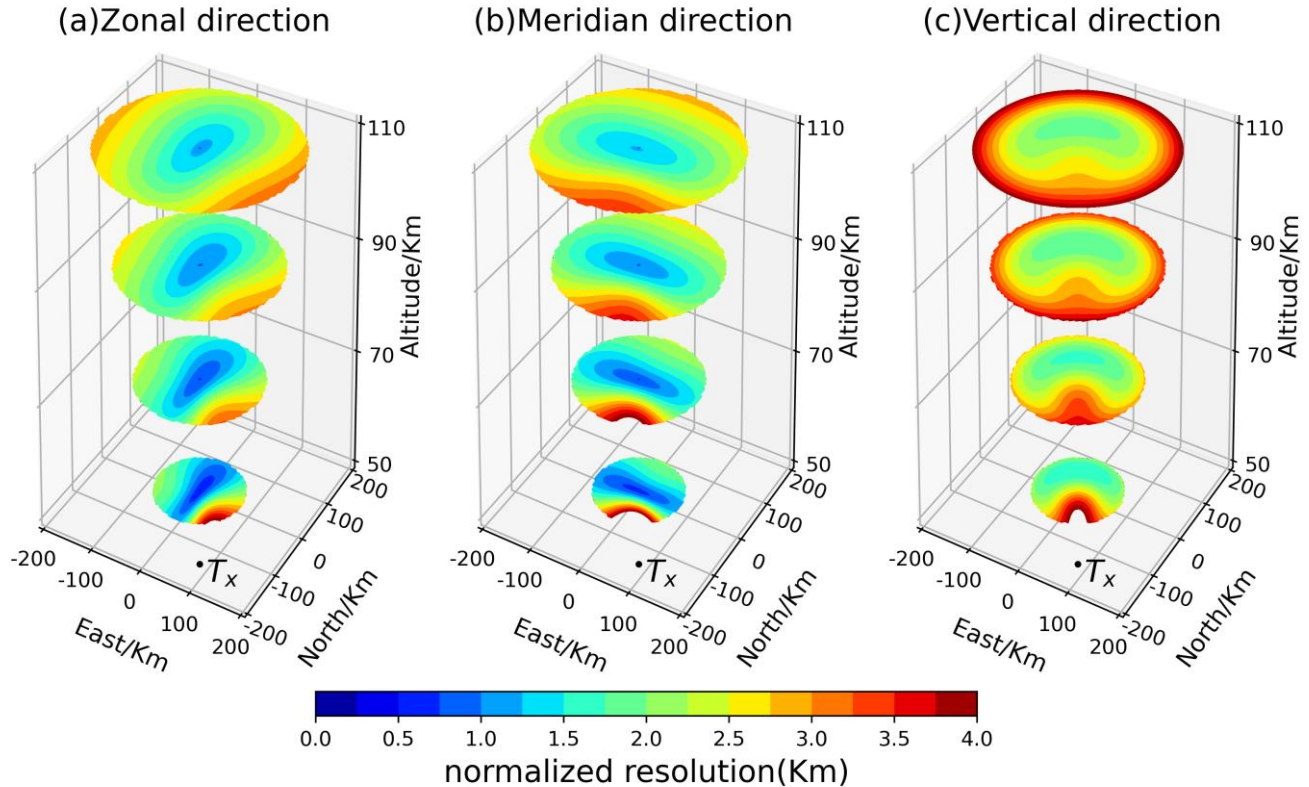


Figure 7: the normalized vertical resolution distribution using the analytical method in this paper. The first and second row represent a vertical section from height 50 km to 120 km. The third row represent the horizontal section in 90 km and the receiver is on the origin with positive coordinate value represent east or north direction. The first row has the same parameters settings as Figure 6 and is used to compare with Figure 6. E_1 related resolution will change with transmitter/receiver configuration because it consider the error term “ δR_s ”. Thus, the total vertical resolution will change with transmitter/receiver configuration. With transmitter/receiver distance varying from 300 km (the

first row) to 150 km (the second row), the total vertical resolution distribution is changed. The third row is the perspective to the horizontal section in 90 km altitude for the second row. The normalized resolution values exceed 3 km aren't shown.

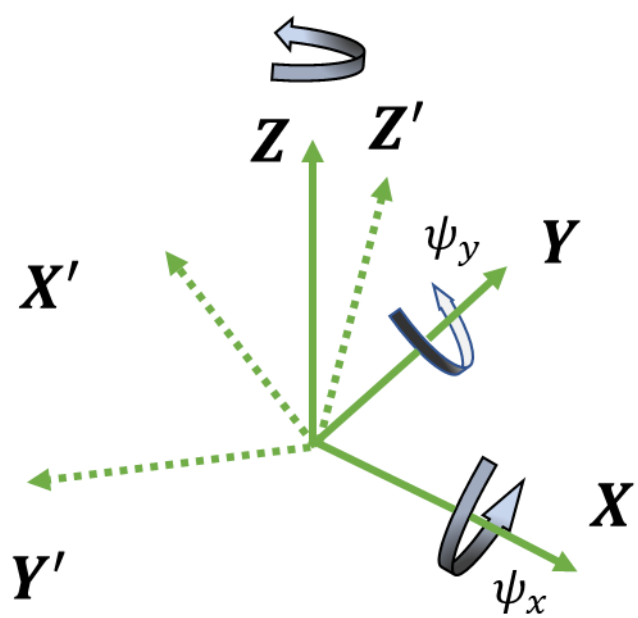
665

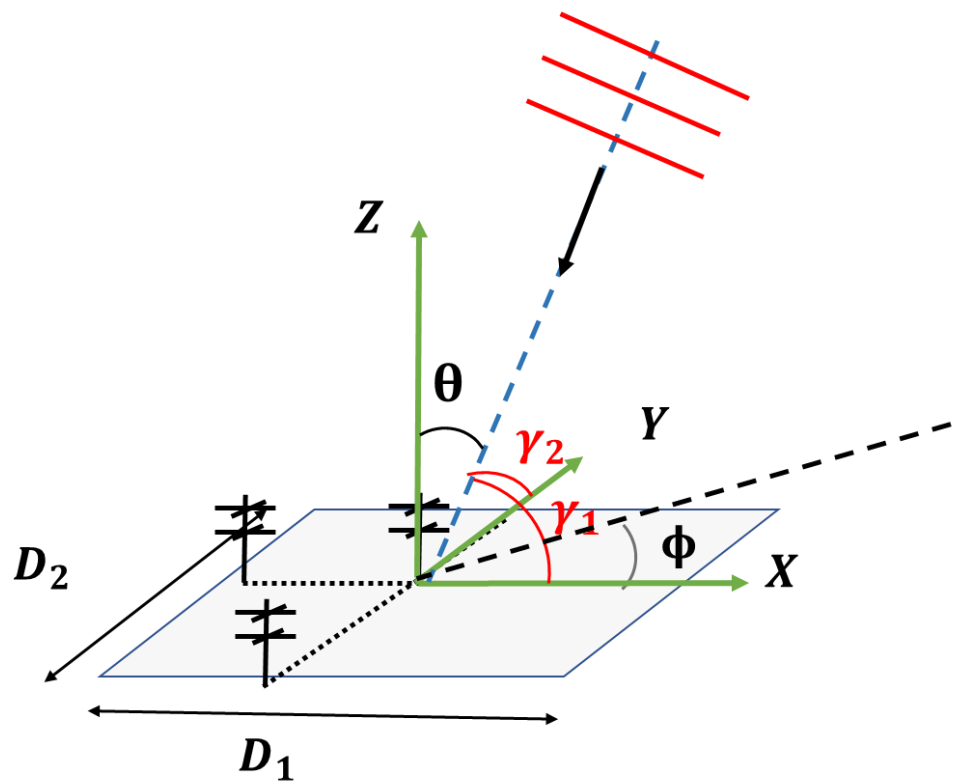


670

Figure 8 the 3D contour plot of normalized resolution distribution for a multistatic radar link whose baseline length is 180 km and transmitter is south by east 30° of the receiver. The black dots represent the position right above transmitter and the receiver is on the origin of axes. (a), (b) and (c) are the normalized resolution distribution in zonal, meridian and vertical respectively. The subplot's four slice circle from bottom to top are the horizontal section in 50 km, 70 km, 90 km and 110 km height. The region whose elevation angle of the receiver is less than 30° isn't shown and therefore the slice circles become larger from the bottom to the top. The normalized resolution values exceed 4 km which correspond 16 km resolution aren't shown.

675





Receiver

685 Figure A.2 (two antennas are not shown for concise)